Quantification of Mitochondrial Membrane Potential in the Isloated Rat Lung Using R6G

Anthony Cammarata
Marquette University

QUANTIFICATION OF MITOCHONDRIAL MEMBRANE POTENTIAL IN THE ISOLATED RAT LUNG USING R6G

By

Anthony Cammarata, B.S.

A thesis submitted to the Faculty of the Graduate School, Marquette University, in Partial Fulfillment of the Requirements for the Degree of Master of Science

Milwaukee, Wisconsin

December 2019

ABSTRACT
QUANTIFICATION OF MITOCHONDRIAL MEMBRANE POTENTIAL IN THE ISOLATED RAT LUNG USING R6G

Anthony Cammarata, B.S.

Marquette University, 2019

Mitochondrial membrane potential ($\Delta\psi_m$) plays a key role in vital mitochondrial functions, and its dissipation is a hallmark of mitochondrial dysfunction in various cell types. The objective of this study was to develop an experimental and computational approach for estimating $\Delta\psi_m$ in intact rat lungs using the lipophilic fluorescent cationic dye rhodamine 6G (R6G).

Rat lungs were isolated and connected to a ventilation-perfusion system. The experimental Protocol consisted of three single-pass phases: loading, wash, and uncoupling, in which the lungs were perfused with R6G-containing perfusate, fresh R6G-free perfusate, or R6G-free perfusate containing the mitochondrial uncoupler FCCP, respectively. This Protocol was carried out with or without lung perfusate containing verapamil, an inhibitor of the multi-drug efflux pump P-glycoprotein.

Results show that the addition of FCCP resulted in an increase in R6G venous effluent concentration, and that this increase was larger in the presence of verapamil than in its absence. A physiologically based pharmacokinetic (PBPK) model for the pulmonary disposition of R6G was developed and used for quantitative interpretation of the kinetic data, including estimating $\Delta\psi_m$. The estimated value of $\Delta\psi_m$ (-139 ± 21 (SD) mV and -128 ± 14 mV without and with verapamil, respectively) is consistent with that estimated previously in cultured pulmonary endothelial cells. These results demonstrate the utility of the proposed approach for quantifying $\Delta\psi_m$ in intact functioning lungs.

This approach has potential to provide quantitative assessment of the effect of injurious conditions on lung mitochondrial function, and to evaluate the impact of therapies that target mitochondria.

ACKNOWLEDGEMENTS

Anthony Cammarata, B.S.

First and foremost, I would like to thank my advisor, Dr. Said Audi, whose mentorship and expertise have made my studies possible. His guidance throughout my career at Marquette University has been vital in both my academic and professional life. It wasn't always the easiest path for the two of us because we hit many unexpected roadblocks in trying to complete this thesis. I want to express my genuine appreciation for his patience and understanding through it all.

Also, I would like to give a sincere thanks to Dr. Anne Clough, Dr. Elizabeth Jacobs, and Dr. Ranjan Dash for serving on this thesis committee. I wish to extend my gratitude to Mr. Carlos Marquez-Barrientos and Ms. Lucy Hatfield for their help with the experiments and lab work.

I dedicate this Thesis to my wonderful family members, who have continuously provided me with unwavering support and love. To my Mom, my Dad, Linda, and Gina I can honestly say that without you guys that this work would not have been possible. Between all the late night phone calls from me when I was stressed out and just the general encouragement you guys gave me I am eternally thankful. I would like to formally thank them for all they do for me and continue to do for me.

To my rock, my muse, my motivation, and my love Jess. If it wasn't for your continuous and sometimes annoyingly positive attitude and belief in me I do not know where I would be right now in both my personal and professional life. Through all the ups and downs you supported me both financially and emotionally. I can never repay you for what you have done for me I only ask that you can find the patience to allow me to try and repay you now and forever. Thank you for all you have done.

Lastly, I want to thank Marquette University for the opportunity to earn my bachelor's and master's degrees and to work on this project. Finally, for anyone who has contributed, directly and indirectly, to the completion of this thesis, I extend my appreciation.

TABLE OF CONTENTS

LIST OF TABLES

LIST OF FIGURES

CHAPTER 1: INTRODUCTION, BACKGROUND, AND OBJECTIVE

1.1 Clinical Motivation

Mitochondria are commonly known as the powerhouse of the cell. For pulmonary endothelial cells, mitochondria produce approximately 80-85% of ATP needed for cellular functions (Bongard et al., 2013; Fisher AB et al., 1984). Mitochondria are also implicated in other important cellular functions, including apoptosis, calcium regulation, nitric oxide signaling, and are a primary source of reactive oxygen species (ROS) under physiological and pathophysiological conditions (Carraway et al., 2008; Sepehr et al., 2013; Murphy et al., 2009; Bongard et al., 2013; Gan et al., 2011). Mitochondrial membrane potential ($\Delta\psi_m$) is a major component of the mitochondrial electrochemical transmembrane potential (proton motive force), which plays a key role in vital mitochondrial bioenergetics, metabolic, and signaling functions (Gan et al., 2011; Duchen et al., 2003). In addition, mitochondrial dysfunction has been implicated in the pathogenesis of acute and chronic lung diseases (Audi et al., 2017; Fu et al., 2017; Ten et al., 2019; Ryter et al., 2018; Piantadosi et al., 2017; Audi et al., 2005; Sepehr et al., 2013). Thus, the ability to quantify $\Delta\psi_m$ in an intact functioning lung is essential to further the understanding of the role of mitochondrial dysfunction in the pathogenesis of lung injury and diseases, and to assess the efficacy of potential therapies that target the mitochondria.

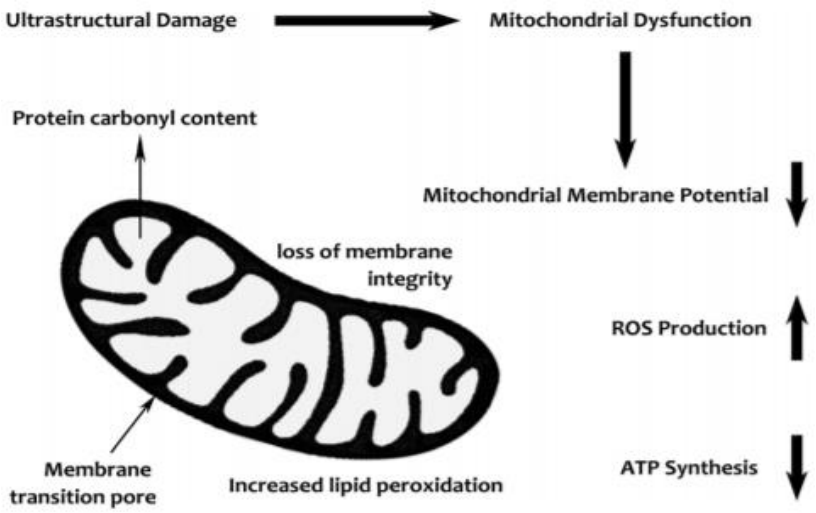

Figure 1.1: Mitochondrial Dysfunction. This schematic shows how a decrease in mitochondrial membrane potential due to mitochondrial structural damage causes a decrease in ATP production and an increase in ROS production (Taken from Morris et al., 2015 with permission).

1.2 Mitochondrial Membrane Potential: Electrochemical Gradient, ATP Production via Oxidative Phosphorylation

For lung tissue, glucose is by far the most oxidizable substrate under physiological conditions (Bonora et al., 2012). The development of $\Delta\psi_m$ and the synthesis of most mitochondrial ATP in the lung tissue start with the cellular uptake of glucose, followed by glycolysis and uptake of pyruvate into the citric acid or tricarboxylic acid (TCA) cycle, and ends with oxidative phosphorylation. During glycolysis, glucose is converted into two ATP, two NADH, and two pyruvate molecules, through a series of chemical reactions. The two pyruvate molecules then enter the TCA cycle where they are converted into two CO_2 molecules, two ATP molecules, three NADH molecules, and one $FADH_2$ molecule. Lastly the $FADH_2$ and NADH molecules are reduced to NAD^+ and FAD to provide energy for the electron transport chain (ETC) in the form of electrons. The electrons that are produced create an electrochemical gradient. The transfer of

electrons in the ETC (complexes I-IV) makes it possible for protons to be pumped (at complexes I, III, and IV) against their concentration gradient, across the inner mitochondrial membrane, and into the mitochondrial intermembrane space. Hence, generating a proton gradient and furthermore generating a membrane potential across the inner mitochondrial membrane. The energy that is generated via the proton motive force (proton gradient and membrane potential) then drives the formation of 34 ATP from ADP at complex V. This process accounts for ~80-85% of ATP production in lung tissue. It should be noted that the total molecules of ATP created per glucose molecule is approximately 38. Therefore, a change in $\Delta\psi_m$ is indicative of a change in lung tissue bioenergetics and mitochondrial function (Perry et al., 2011; Bonora et al., 2012).

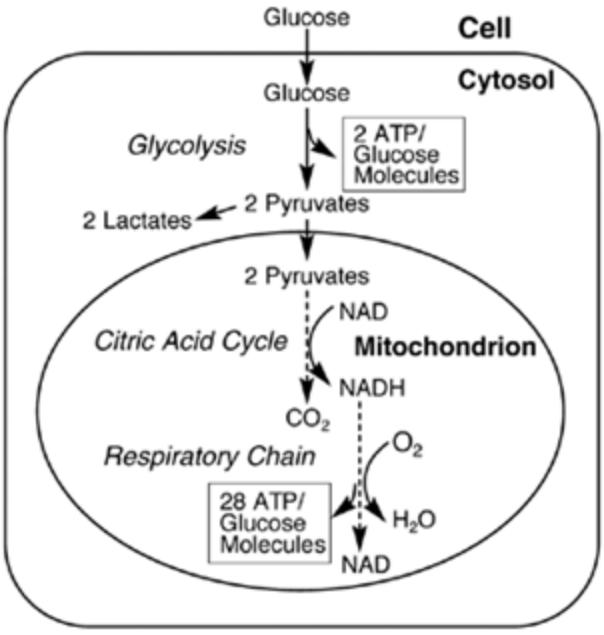

Figure 1.2: Cellular Bioenergetics. Schematic of the three main cellular processes (glycolysis, TCA cycle, and oxidative phosphorylation) that are involved in the conversion of glucose to ATP (Taken from Cunningham et al., 2004 with permission).

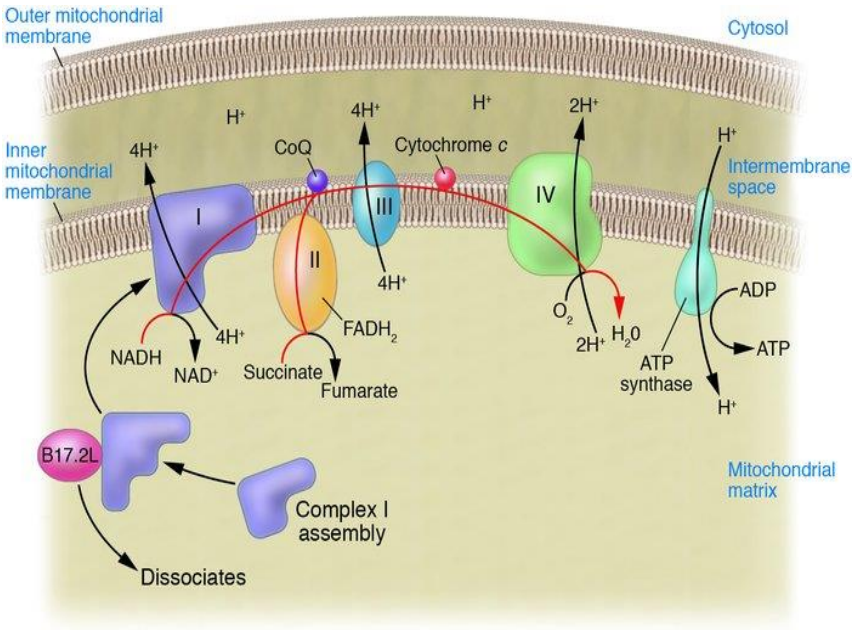

Figure 1.3: Mitochondrial ETC and ATP Synthesis Schematic Representation. The four complexes of the ETC are shown as well as ATP synthase. The ETC is important in regulating membrane potential (Taken from Nussbaum et al., 2005 with permission).

Dissipation of $\Delta\psi_m$ is a hallmark of mitochondrial dysfunction observed in various cell types, including pulmonary endothelial cells exposed to oxidative stress (Gan et al., 2011; Ma et al., 2018; Merker et al., 2009; Ruchko et al., 2005). Regulation of $\Delta\psi_m$ is very important, not only for ATP production, but also for the transport of metabolites and ions in and out of the cells. $\Delta\psi_m$ also has a large influence on the importing of precursors for enzymes and mitochondrial protein synthesis (Chen et al., 1988). Therefore, conditions that alter $\Delta\psi_m$ could lead to mitochondrial dysfunction. Hence, the ability to quantify $\Delta\psi_m$ is critical for understanding the pathogenesis of lung diseases for which mitochondrial dysfunction is a key factor. It is also important for the evaluation of the efficacy of novel therapies that target mitochondrial function.

1.3 Methods for Measuring Mitochondrial Membrane Potential

Fluorescent lipophilic cations such as rhodamine dyes have been used for monitoring $\Delta\psi_m$, predominantly in reduced systems, including cultured cells and isolated mitochondria (Gan et al., 2011; Fu et al., 2017; Farkas et al., 1989; Perry et al., 2011; Aiuchi et al., 1982; Johnson et al., 1981; Scaduto et al., 1999). For most studies, this involved measurement of the intensity of fluorescent dyes within cultured cells or isolated mitochondria. Such measurements are confounded by the propensity of the dyes to undergo self-aggregation and quenching due to accumulation in mitochondria and cytosol (Gan et al., 2011).

A study by Perry et al. included the development of a guide for using cationic probes for assessing $\Delta\psi_m$ (Perry et al., 2011). The study provides an overview of cationic dyes that have been used to measure membrane potential, including TMRM, TMRE, and R123. The study also provides a step by step description on how cationic probes can be used properly to assess $\Delta\psi_m$.

Previous studies have demonstrated the utility of cationic rhodamine dyes, including rhodamine 6G (R6G), to probe $\Delta\psi_m$ mostly in isolated mitochondria and cultured cells (Gan et al., 2011; Scaduto et el., 1999; Johnson et al., 1981; Baracca et al., 2003; Farkas et al., 1989; Mandalà et al., 1999; Aiuchi et al., 1982; Ehrenberg et al., 1988; Gear et l., 1974; Solaini et al., 2007). Mandalà et al. used R6G as a probe for plasma membrane potential in cultured bovine aortic endothelial cells (Mandalà et al., 1999). They reported a linear relationship between the fluorescence intensity (F.I.) and the plasma membrane potential. The value of F.I. dropped following the addition of an inflammatory mediator and mitochondrial uncoupler (bradykinin), an ionophore

(nigericin), and/or the sodium-potassium ion pump inhibitor ouabain to the medium surrounding the cells. However, the addition of mitochondrial inhibitors (myxothiazol and oligomycin) to the medium did not affect F.I., which may suggest that R6G is not sensitive enough to changes in $\Delta\psi_m$ (Mandala et al., 1999). However, other studies have shown that R6G is a mitochondrial specific dye and therefore can provide a measure of $\Delta\psi_m$ (Johnson et al., 1981; Farkas et al., 1989). For instance, Johnson et al. performed a study in which they monitored the relative $\Delta\psi_m$ in living cells using cationic dyes including Rhodamine 123 (R123) and R6G. The results indicate that the fluorescence intensities associated with mitochondria were reflections of $\Delta\psi_m$ (Johnson et al., 1981). R6G was also used to evaluate $\Delta\psi_m$ in rat brain synaptosomes (Aiuchi et al., 1982). They demonstrated that R6G emission signal increased when depolarizing agents were added to the synaptosome suspension medium. In addition, the authors developed a modified Nernst equation that allows for the conversion of changes in R6G emission signal to membrane potential in mV (Aiuchi et al., 1982). Ehrenberg et al. also demonstrated the utility of cationic dyes, including R6G, to probe membrane potential in various types of cultured cells (Ehrenberg et al., 1988). These studies clearly demonstrated the utility of R6G probing $\Delta\psi_m$ in isolated mitochondrial and cultured cells.

Huang et al. performed a study in which they developed a model that allowed them to better understand the relationship between $\Delta\psi_m$ and measured fluorescence using the cationic dye R123 (Huang et al., 2007). They performed experiments in isolated cardiac mitochondria, and developed a computational model for quantitative interpretation of the resulting kinetic data. The model they used incorporated dye flux across a membrane as well as dye self-quenching. This was then added to a model of

mitochondrial electrophysiology which was used to estimate various parameters from the measured kinetic fluorescence data, including $\Delta\psi_m$.

Gan et al. developed an experimental and computational approach for estimating mitochondrial and plasma (cellular) membrane potentials in cultured pulmonary arterial endothelial cells based on the extracellular disposition of the rhodamine dye tetramethyl rhodamine ethyl ester perchlorate (TMRE) and rhodamine 123 (R123) following its addition to the surrounding medium (Gan et al., 2011). Unlike other studies with cultured cells, Gan et al. evaluated the cellular uptake of each dye by measuring changes in its concentration in the surrounding medium instead of the concentration in cells (Gan et al., 2011). For quantitative interpretation of the measured kinetic data, they developed a computational model that accounted for the dominant processes that determine the uptake of each dye, including plasma and mitochondrial membrane potentials and the multi-drug efflux pump P-glycoprotein (Pgp) for which TMRE and R123 are substrates (Gan et al., 2011). Pgp pumps rhodamine dyes from the cytoplasm back into the surrounding medium. The objective of the present study was to develop a similar experimental and computational approach for estimating $\Delta\psi_m$ in isolated perfused rat lungs using the lipophilic fluorescent cationic dye rhodamine 6G (R6G).

Our choice of R6G for this study was motivated in part by the work of Roerig et al. who demonstrated significant R6G uptake and retention in isolated perfused rabbit lungs (Roerig et al., 2004), and by R6G's high permeability in cell membranes of several types of cells, including pulmonary endothelial cells (Mandala et al., 1999).

Scaduto et al. attempted to probe $\Delta\psi_m$ in the intact heart by monitoring the surface emission fluorescent of Tetramethylrhodamine Methyl Ester Perchlorate (TMRM)

(Scaduto et al., 1999). Recirculated TMRM in perfusate was taken up and retained in the heart tissue. However, the results with mitochondrial uncouplers were difficult to interpret in part because of alteration in the fluorescent properties of TMRM in heart tissue due to the accumulation of TMRM in mitochondria. The experimental and computational approach described in this thesis overcomes this limitation by estimating the lung uptake and accumulation of R6G from the lung inlet and outlet R6G concentrations on passage through the pulmonary circulation instead of from lung surface measurements, and by using a computational PBPK model to account for the dominant, various vascular and tissue processes that determine the lung uptake and accumulation of R6G, including $\Delta\psi_m$.

1.4 Objective and Specific Aims:

Previous studies have quantified $\Delta\psi_m$ predominately in isolated lung tissue mitochondria and to lesser extent in cultured lung cells using various cationic dyes, including rhodamine dyes (Gan et al., 2011; Scaduto et al., 1999; Perry et al., 2011; Chen et al., 1988; Johnson et al., 1981; Davis et al., 1985; Baracca et al., 2003; Huang et al., 2007; Mandala et al., 1999; Aiuchi et al., 1982). Studies using these reduced systems are useful and provide important information which allows for the application of several tools of cell biology that are not applicable at the organ level. However, they cannot reproduce the multicellular environment in an intact functioning lung under physiological and pathophysiological conditions. Therefore, an approach for quantifying $\Delta\psi_m$ in an intact functioning lung is needed. Thus, the **objective** of this thesis was to develop an experimental and computational approach for estimating $\Delta\psi_m$ in isolated perfused rat lungs using the cationic fluorescent dye R6G. Thus, the specific aims of the thesis are to:

Aim # 1: evaluate the pharmacokinetics of R6G uptake in isolated perfused rat lungs. For this aim, experiments were carried out under different experimental conditions to identify the dominant processes that determine the uptake and retention of R6G on passage through the pulmonary circulation, and the sensitivity of R6G lung uptake to changes in $\Delta\psi_m$.

Aim # 2: Develop a physiologically-based pharmacokinetic (PBPK) model for mechanistic and quantitative interpretation of the R6G spectroscopy kinetic data during passage through the rat pulmonary circulation. The lung uptake and retention of R6G on passage through the pulmonary circulation is the net result of multiple tissue and vascular processes, and hence estimating the mitochondrial membrane potential $\Delta\psi_m$ or a change in $\Delta\psi_m$ from the measured kinetic data is not straight forward. Thus, for this aim we developed a PBPK computational modeling for estimating parameters descriptive of those processes, including $\Delta\psi_m$, from the differences between lung inlet and outlet perfusate R6G concentrations under different experimental conditions.

The results of the present study demonstrate the utility of the described experimental and computational approach for quantifying $\Delta\psi_m$ in isolated perfused lungs.

CHAPTER 2: EXPERIMENTAL METHODS

2.1 Materials

Rhodamine-6G (R6G), verapamil hydrochloride, Carbonyl cyanide 4-(trifluoromethoxy) phenylhydrazone (FCCP), and all other reagents that are used in experiments were purchased from Sigma-Aldrich (St. Louis, MO).

2.2 Isolated, Perfused Rat Lung Preparation

Animal Protocols described below were approved by the Institutional Animal Care and Use Committees of the Veterans Affairs Medical Center and Marquette University (Milwaukee, WI).

Adult male Sprague-Dawley rats (348 ± 3 g (SE), n = 59) were used for this study. Each rat was anesthetized with sodium pentobarbital (40-50 mg/kg intraperitoneal). The trachea was surgically isolated and cannulated, the chest opened and heparin (0.7 IU/g body wt.) injected into the right ventricle as previously described (Audi et al., 2018). The pulmonary artery and the pulmonary venous outflow were accessed via cannulas, then the heart/lungs were removed and connected to a ventilation-perfusion system.

The Krebs-Ringer bicarbonate perfusate contained (in mM) 4.7 KCl, 2.51 $CaCl_2$, 1.19 $MgSO_4$, 2.5 KH_2PO_4, 118 NaCl, 25 $NaHCO_3$, and 5.5 glucose. The perfusate also contained 0.5% to 3% bovine serum albumin (BSA) plus 2.5% to 0% Ficoll to maintain consistent oncotic pressure. The perfusion system was primed with the perfusate maintained at 37^{o}C and equilibrated with 15% O_2, 6% CO_2, balance N_2 gas mixture resulting in perfusate PO_2, PCO_2 and pH of ~105 Torr, 40 Torr, and 7.4, respectively.

The lung was ventilated (40 breaths/min) with the above gas mixture with end-inspiratory and end-expiratory pressures of ~ 6 and 3 mmHg, respectively. The pulmonary artery and airway pressures were referenced to atmospheric pressure at the level of the left atrium and monitored continuously during the experiments. Perfusate was pumped (5 to 20 ml/min) through the lung until it was evenly blanched and venous effluent was clear of visible blood before switching from single pass to recirculation mode.

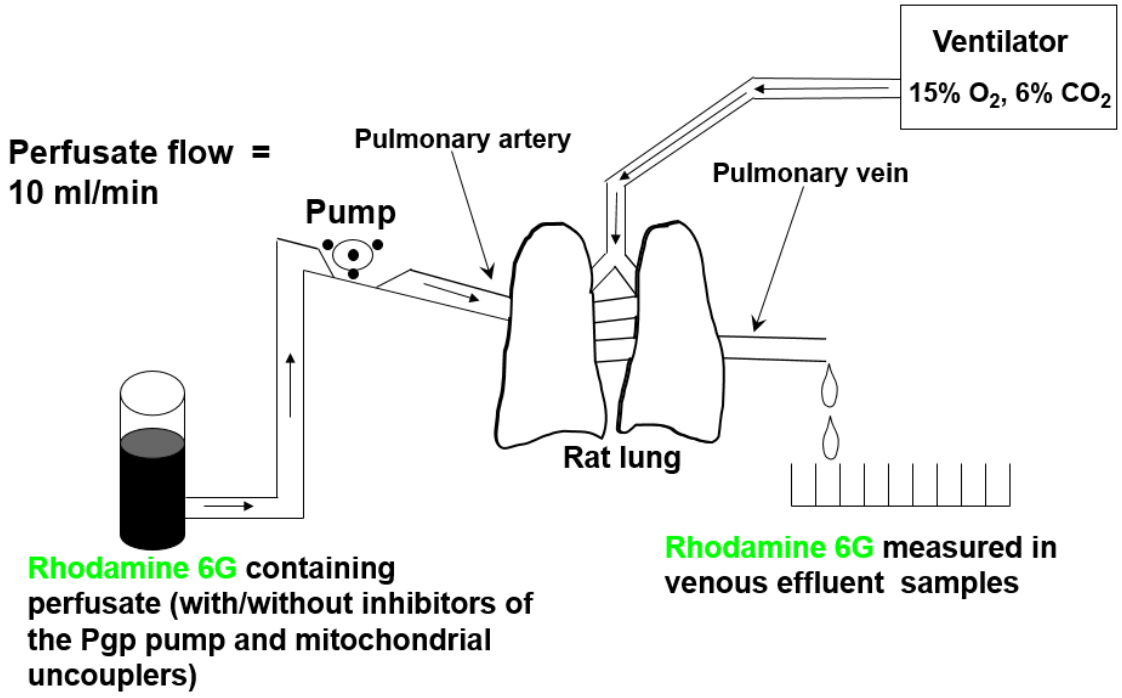

Figure 2.1: *Schematic of the Ventilation-Perfusion system used for IPL experiments.*

2.3 Hyperoxia treatment:

Rat exposure to high oxygen environment (hyperoxia is a well-established animal model of clinical acute lung injury(Audi et al., 2005; Audi et al., 2016). Rats were placed in a sealed, temperature controlled, acrylic chamber 59 L chamber (33.0 × 58.3 × 30.5 cm) and exposed to >95% oxygen (n = 2) for 48 hours. Within the chamber, carbon

dioxide levels were maintained at <0.5%, and temperature was maintained at 20-22°C. The rats were exposed to a 12:12 hours light-dark cycle. The O_2 and CO_2 levels were monitored to ensure the desired O_2 concentration was achieved. This Protocol has been approved by the Institutional Animal Care and Use Committees of the Veterans Affairs Medical Center and Marquette University (Milwaukee, WI).

2.4 Optical Imaging Systems

The RatioMaster fluorescence imaging system (Photon Technology International, HORIBA Scientific) was used to measure the R6G fluorescence (Figure 2.2). It uses a xenon bulb as the light source and is operated and controlled using custom software (FelixGX-4.3.2010) which is run using a windows operating system. For R6G, the monochromator was set to an excitation wavelength of 525 nm. The emission filter used (Chroma Technology Corporation, Bellows Falls, Vermont part # AT565/30m) has a wavelength of 565 ± 15 nm.

Figure 2.2: PTI System used to gather experimental data

Table 2.1: Inhibitors and Uncouplers and their Target Sites.

Effects of Inhibitors and Uncouplers	
P-trifluoromethoxy carbonyl-cyanide phenyl-hydrazone (FCCP)	– Protonophore: uncouples the mitochondrial membrane potential by increasing the membrane's permeability to protons. – Low concentrations depolarize the mitochondrial membrane while high concentrations may also depolarize the plasma membrane (Perry et al., 2011)
Verapamil hydrochloride	– Inhibitor of the plasma membrane Pgp pump.

2.5 Experimental Protocols

Protocol 1: *Effect of R6G input concentration, pump flow, and perfusate % BSA on R6G extraction on passage through the lungs.*

For this Protocol, the objective was to assess the impact of R6G infused concentration, perfusate flow, perfusate % BSA, and connecting tubing from the perfusate reservoir to the lungs on R6G uptake on its passage through the pulmonary circulation.

For the first set of experiments (n = 7), the perfusate included 0.5% BSA and 2.5% Ficoll. Once the lungs were clear of blood, the pump was stopped, and the reservoir emptied and then refilled with 120 ml of perfusate. Two 1 ml reservoir samples were collected before and after the addition of R6G for a final concentration of 0.25 μM. Those samples were used to determine the background signal and the actual R6G concentration in the reservoir. During the 10 minute lung perfusion (single pass mode) with the R6G-containing perfusate, two 1-ml lung venous effluent samples were collected every 20 seconds for the first 5 minutes and every minute for the last 5 minutes, with the first sample collected at time 40 seconds, where t = 0 seconds was the start of the loading phase. Based on the volume (~ 4 ml) of the system (lung + tubing) and flow, one would

expect no R6G signal in the venous effluent samples collected prior to 40 seconds. Samples were then centrifuged for 1 min (13,000 g, 4°C) to remove any cellular components and debris. The sample supernatant was then transferred into a plastic cuvette and its 565 nm emission signal (525 nm excitation) was measured using a RatioMaster fluorescence system (Photon Technology International, HORIBA Scientific, NJ) (Audi et al., 2018). The emission filter was centered at 565 nm (ET565/30M, Chroma, VT) with a bandwidth of 30 nm. R6G optical density was determined and converted to concentration using a standard curve. The lung R6G extraction ratio (ER), a measure of the fraction of the input extracted on passage through the lungs, was determined using the following equation

$$ER = 1 - \frac{[C_v]}{[C_{in}]} \tag{2.1}$$

where $[C_v]$ is the R6G venous effluent concentration and $[C_{in}]$ is the infused R6G concentration (0.25 μM).

For some experiments (n = 3), the above Protocol was repeated with no lungs attached to the ventilation-perfusion system to assess the impact of the tubing connecting the reservoir to the lungs on the concentration of R6G in the venous effluent.

Based on results from the above experiments (see *Results* section), it was determined that the R6G concentration in the venous effluent approached steady state at ~6 min at a pump flow of 10 ml/min. Thus, for subsequent experiments under Protocol 1, venous effluent was collected only 6 min after the start of the pump for a flow of 10 ml/min, and only 3 min and 12 min after the start of the pump for flows of 5 ml/min and 20 ml/min, respectively.

Using the above Protocol with flow of 10 ml/min, we assessed the impact of R6G input (reservoir) concentration (0.125, 0.5, or 1.25 μM) on R6G ER on passage through the pulmonary circulation. For 0.5 μM and 1.25 μM, venous effluent samples were first diluted with perfusate before measuring the emission signal to keep the intensity within the dynamic range of the fluorescence measuring system. In addition, we assessed the impact of changing perfusate % BSA (1%, 2%, or 3%) on R6G ER at 10 ml/min. For perfusate with BSA concentration of 1, 2 or 3%, the Ficoll concentration was 2%, 1% and 0%, respectively, to maintain constant oncotic pressure.

Using the above Protocol with perfusate of 0.5 % BSA and R6G reservoir concentration of 0.25 μM, we assessed the impact of pump flow (5 ml/min or 10 ml/min) on R6G ER on passage through the pulmonary circulation.

At the end of the above Protocol, the lungs were removed from the system and their wet weight was measured. The lungs were then dried, and the dry weight was measured.

Protocol 2: *Effect of treating isolated perfused lungs with verapamil and/or FCCP on R6G venous effluent concentration.*

Based on results from Protocol 1 (see *Results* section), the following experimental conditions were used for Protocol 2: perfusate with 0.5% BSA +2.5% Ficoll, 10 ml/min pump flow, and 0.25 μM R6G reservoir concentration. These conditions result in lung steady-state ER of ~ 0.5, halfway within the dynamic range (0 to 1) of ER.

Protocol 2 consisted of three single-pass perfusion phases: The *loading phase* in which the lungs were perfused with R6G-containing perfusate, the *wash phase* in which the lungs were perfused with fresh perfusate with no R6G, and the *uncoupled phase* in

which the lungs were perfused with perfusate containing the uncoupler FCCP and no R6G. Once the lungs were visually clear of blood, the flow was stopped to empty the perfusate in the reservoir and refilled with 120 ml of fresh perfusate. Before mixing the perfusate with the R6G, two 1-ml samples were collected to provide background signal for the loading phase. R6G stock (41.8 μM) was then added to the perfusate in the reservoir for a final concentration of ~0.25 μM. Two 1-ml samples were then collected from the reservoir to provide a measure of actual R6G lung input concentration for the loading phase. The remaining perfusate was used to perfuse the lungs during the 10 minute loading phase. During this phase, two 1-ml lung venous effluent samples were collected every 20 seconds for the first 5 minutes and every minute for the last 5 minutes, with the first sample collected 40 seconds after the start of the loading phase.

At the end of the loading phase, the pump was stopped, and the reservoir quickly emptied and then refilled with R6G-free perfusate that was used to perfuse the lungs during the 3-minute wash phase. Prior to restarting the pump for the wash phase, two 1-ml samples were collected from the reservoir and used as background samples for the wash phase. During the wash phase, two 1-ml venous effluent samples were collected every minute.

At the end of the wash phase, the pump was stopped again, and the reservoir emptied and then refilled with 75 ml of R6G-free perfusate containing the uncoupler FCCP at a concentration of 67 μM. This concentration is high enough to ensure maximal dissipation of mitochondrial membrane potential (Zhao et al., 2013; Huang et al., 2018). This FCCP-containing perfusate was used to perfuse the lungs during the 7-min uncoupling phase. Prior to starting the pump for the uncoupling phase, two 1-ml samples

were collected to provide background signal. Venous effluent samples were collected every 20 seconds for the first two minutes and then every minute for the last 5 minutes during this phase.

All samples from the three phases of Protocol 2 were centrifuged for 1 min (13,000 g, 4°C) to remove any cellular components and debris. The sample supernatant was then transferred into a plastic cuvette and its 565 nm emission signal (525 nm excitation) was measured (Audi et al., 2018). The R6G emission signal was determined and converted to concentration using a standard curve (see Appendix D).

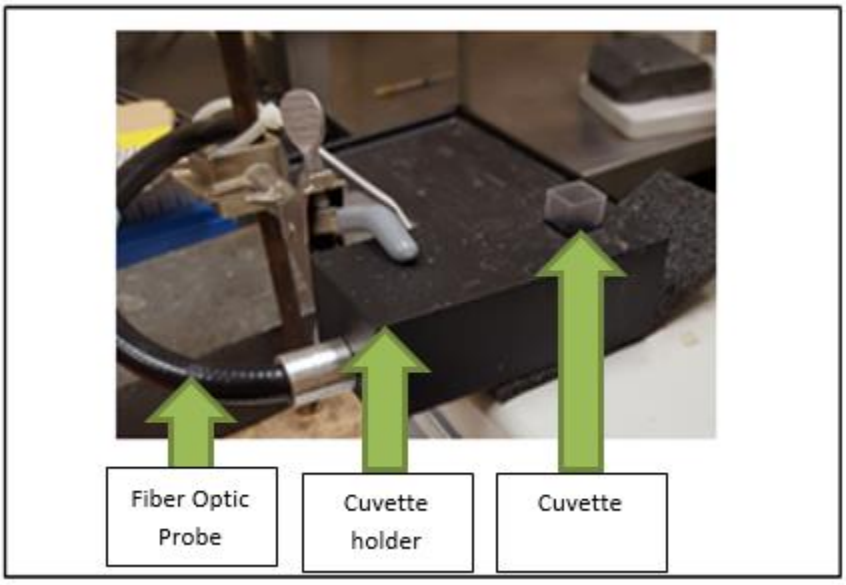

Figure 2.3: Cuvette and Fiber Optic Cable Holder

At the end of Protocol 2, the lungs were removed from the system. Their wet weight was measured, the lungs were dried, and then their dry weight was measured.

2.5.1 Effects of Pgp inhibitors on R6G lung uptake

For a separate group of lungs, the above Protocol was carried out following the inhibition of the Pgp pump that pumps R6G out of the lungs. To inhibit the Pgp pump, Protocol 2 was modified as follows. Prior to the loading phase, perfusate containing verapamil (0.1 mM) Audi et al., 2018) was recirculated through the lungs for 3 minutes at 10 ml/min after which time the flow was stopped, and the reservoir emptied and refilled with perfusate for the loading phase. In addition, perfusate used for all three phases included verapamil (0.1 mM). This concentration is high enough to ensure maximal inhibition of Pgp (Audi et al., 2018; Roerig et al., 2004).

2.5.2 Effects of the uncoupler vehicle, DMSO

FCCP is soluble in dimethyl sulfoxide (DMSO). At high concentrations, DMSO is known to have negative effects (Yuan et al., 2014). Therefore, it was important to know if the concentration DMSO used had any effect on the lung uptake or washout of R6G. To determine the impact of DMSO alone on the lung uptake of R6G, the Protocol was repeated with just DMSO (0.05 % of the perfusate volume) added to the perfusate during the uncoupling phase of Protocol 2.

2.5.3 Standard Curve

For each experimental day, a standard curve was obtained as described below and used to convert R6G emission signal in collected samples to R6G concentration. Six tubes containing perfusate with known concentrations of R6G (0.5 μM, 0.25 μM, 0.125 μM, 0.0625 μM, and 0.03125 μM) were prepared. For each tube, a 2-ml sample was

collected then processed the same way as the samples collected from the lung's venous effluent. Thus, each sample was centrifuged for 1 min (13,000 g, 4°C), after which its 565 nm emission signal was measured. The standard curve was repeated with either verapamil, FCCP, or GF-120918 added to the samples prior to the addition of R6G to determine if the inhibitor/uncoupler and/or its vehicle interfered with the R6G emission signal.

2.6 Effect of rat exposure to hyperoxia on R6G lung uptake:

Protocol 2 was repeated on 2 lungs from rats exposed to >95% O_2 for 48 hours.

2.7 Statistical Analysis

Statistical evaluation of data was carried out using SigmaPlot version 12.0 (Systat Software Inc., San Jose, CA). Values from different groups were compared using unpaired *t*-tests. The level of statistical significance was set at $p < 0.05$. Values are mean ± SE unless otherwise indicated.

CHAPTER 3: EXPERIMENTAL RESULTS

3.1 Rats body weights, lungs wet and dry weights, lungs wet/dry weight ratios, and pulmonary artery pressures:

Table 3.1 shows no significant differences between the body weights, lung wet and dry weights, the wet/dry ratios, and the pulmonary artery pressures of the rats used for Protocols 1 and 2.

Table 3.1: *Body weight, lung wet and dry weight, and wet/dry weight ratio, and pulmonary artery pressure for flow rate of 10ml/min.*

Protocol #	Body weight (g)	Lung wet weight (g)	Lung dry weight (g)	Wet/dry weight ratio	Pulmonary artery pressure (mmHg)
Protocol 1	345.0 ± 2.8 (n = 46)	1.21 ± 0.02 (n = 46)	0.23 ± 0.02 (n = 46)	5.49 ± 0.10 (n = 46)	7.51 ± 0.15 (n = 46)
Protocol 2 (normoxic rats)	365.77 ± 7.8 (n = 13)	1.30 ± 0.03 (n = 13)	0.24 ± 0.01 (n = 13)	5.35 ± 0.06 (n = 13)	6.45 ± 0.24 (n = 13)
Protocol 2 (hyperoxic rats)	325.5 ± 7.42 (n = 2)	1.36 ± 0.07 (n = 2)	0.23 ± 0.01 (n = 2)	5.85 ± 0.004 (n = 2)	5.25 ± 0.88 (n = 2)

Values are mean ± SE.

3.2 Rhodamine-6G (R6G) standard curve for experiments:

Figure 3.1 shows example of the standard curves used to convert R6G emission fluorescent signal to R6G concentration. Neither FCCP (67 μM) nor verapamil (100 μM) had a significant effect on R6G standard curves.

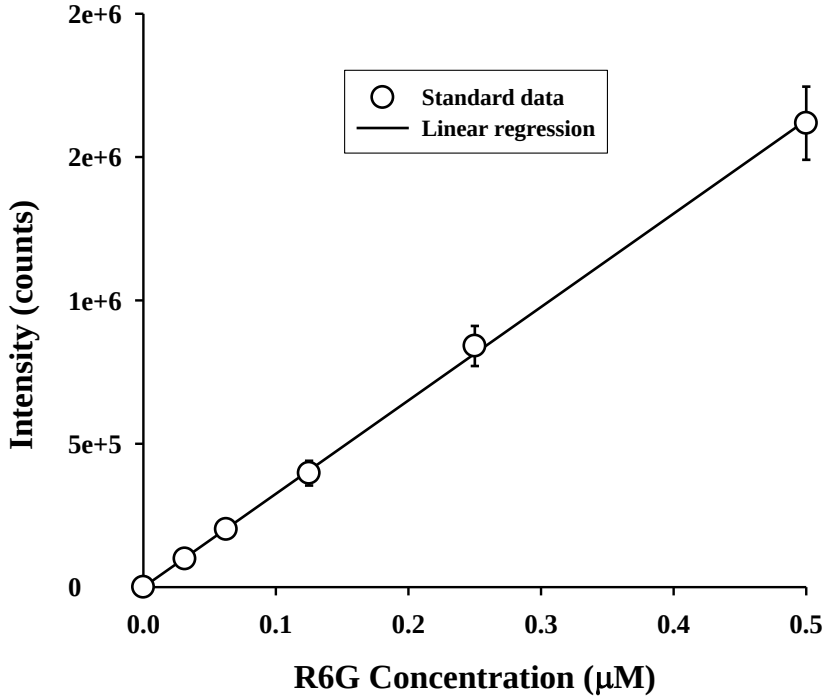

Figure 3.1: Standard curve for R6G. Perfusate BSA concentration was 0.5%. Values are mean ± SE (n = 7).

3.3 Protocol 1: Factors that determine the lung uptake of R6G on passage through the isolated perfused lung

Several factors determine the lung uptake of R6G, including perfusate protein concentration (% bovine serum albumin, or % BSA) and blood flow rate. Figure 3.2 shows R6G ER after 6 min of perfusing lungs with 0.5% BSA perfusate containing 0.125, 0.25, 0.5, or 1.25 μM R6G at flow of 10 ml/min. These results show that for this concentration range, the lung ER is constant (dose-independent) consistent with first-order kinetics for the various vascular and cellular processes that contribute to the lung uptake of R6G.

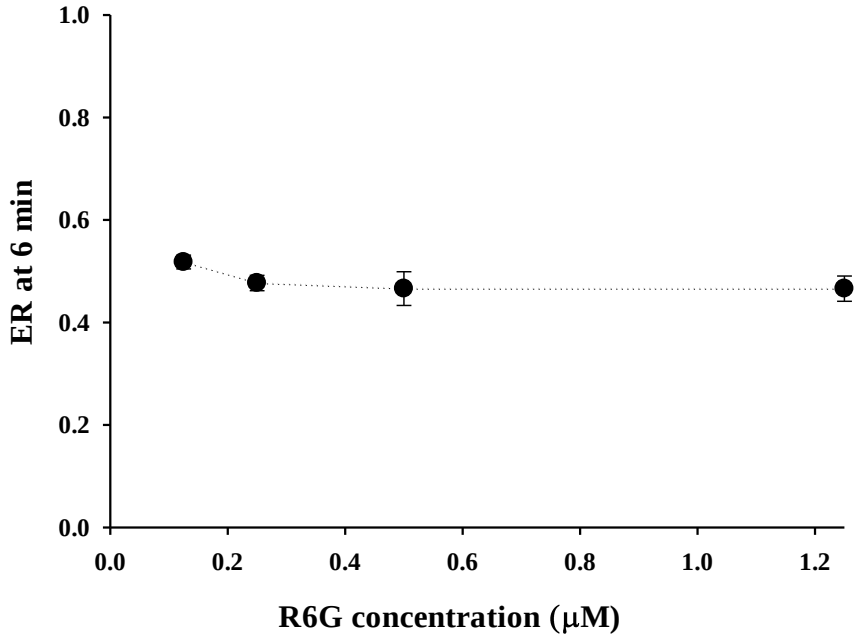

Figure 3.2: R6G lung extraction ratio (ER) after 6 min of perfusion (single pass) as a function of R6G input (reservoir) concentration. Pump flow = 10 ml/min, and perfusate BSA concentration was 0.5%. Values are mean ± SE (n = 6, 7, 4 and 7 for R6G concentrations of 0.125, 0.25, 0.5, and 1.25 μM, respectively).

Figure 3.3 shows R6G ER after 6 minutes of lung perfusion (10 ml/min) with perfusate containing R6G (0.25 μM) and 0.5%, 1%, 2%, or 3% BSA. The results show that ER decreased as the % BSA in perfusate increased, consistent with a decrease in the fraction of R6G that is available for lung uptake.

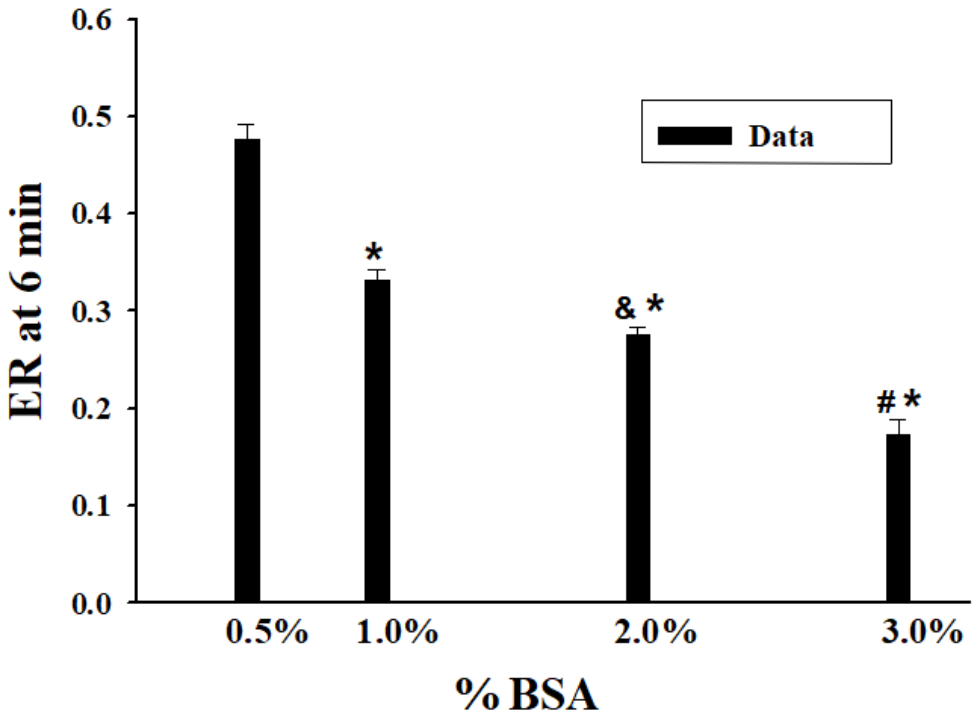

Figure 3.3: R6G lung extraction ratio (ER, solid bars) after 6 min of perfusion (single pass) as a function of perfusate %BSA. Pump flow = 10 ml/min. Values are mean ± SE (n = 10, 3, 3 and 4 for perfusate BSA of 0.5, 1.0, 2.0, and 3.0%, respectively. [*]significantly different from 0.5% BSA ($P < 0.05$, unpaired t-test), [&]significantly different from 1.0% ($P < 0.05$), and [#] significantly different from 2.0% ($P < 0.05$).

Figure 3.4 shows that increasing pump flow (from 5 to 20 ml/min) decreased R6G ER, consistent with a decrease in the time available for R6G uptake. The ER was determined at times of 12 min, 6 min, and 3 min following the start of lung perfusion with R6G-contaning perfusate at flows of 5, 10, and 20 ml/min, respectively.

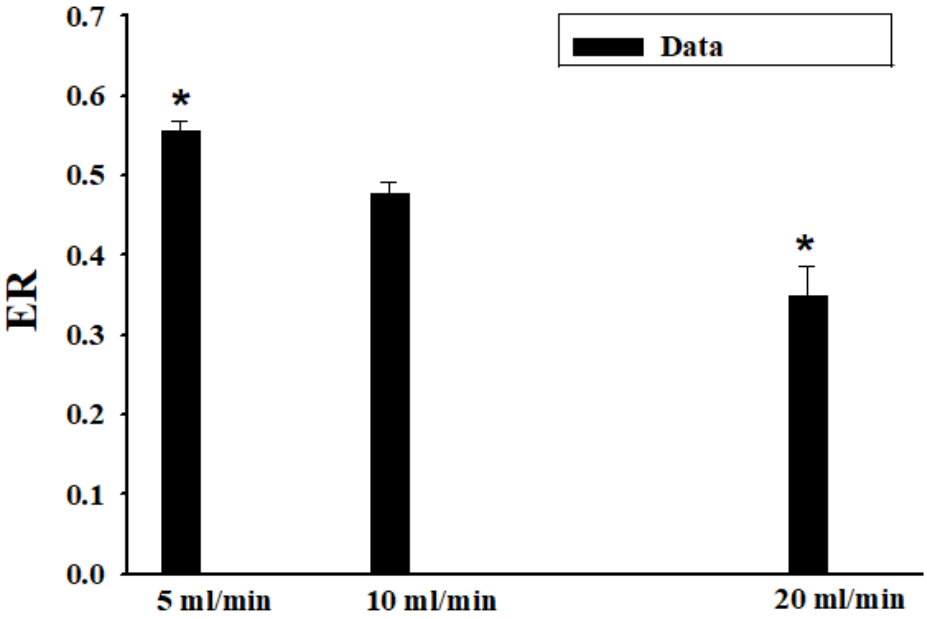

Figure 3.4: R6G lung extraction ratio (ER, solid bars) after 12 min, 6 min, and 3 min of perfusion (single pass) with pump flow set at 5, 10, or 20 ml/min, respectively. Values are mean ± SE (n = 4, 10, and 6 for flow of 5, 10, and 20 ml/min, respectively. *significantly different from ER at flow of 10 ml/min ($P < 0.05$, unpaired *t*-test).

Based on the results in Figures 3.2 – 3.4, we chose the following experiments conditions for Protocol 2: perfusate with 0.5% BSA (and 2.5% Ficoll) and flow rate of 10 ml/min. These conditions result in lung steady state ER of ~ 0.5, halfway within the range (0 to 1) of ER.

Figure 3.5A shows R6G (0.25 μM) ER on passage through the pulmonary circulation at pump flow of 10 ml/min and perfusate containing 0.5% BSA. The results show that ER approaches a steady-state value around 6 min (ER = 0.482 ± 0.013 (SE)) after the start of the perfusion of the lungs with R6G-containing perfusate. Thus at 6 min, ~48% of the infused R6G was extracted or taken up on a single pass through the lungs.

The experimental Protocol for Figure 3.5A was repeated with the lungs removed from the perfusion system. The results in Figure 3.5B show that ER at steady state is not significantly different from zero. Thus, perfusion system tubing is not contributing to R6G ER on passage through the pulmonary circulation.

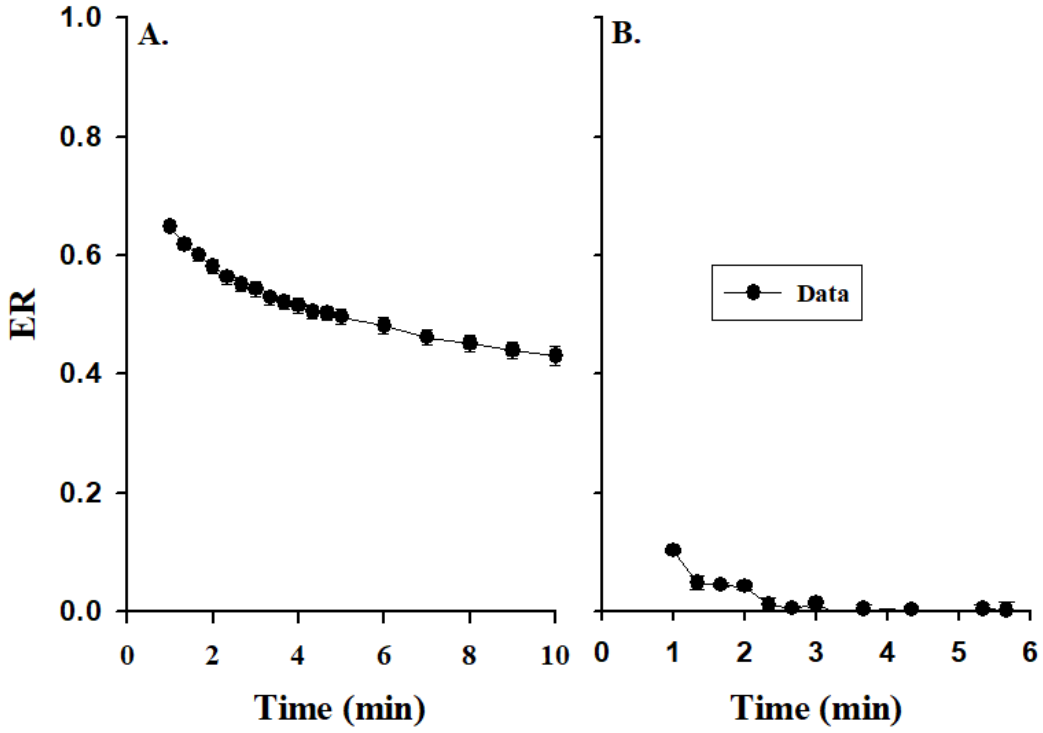

Figure 3.5: *Panel A:* R6G lung extraction ratio (ER) as a function of sampling time on passage through the pulmonary circulation. R6G reservoir concentration was 0.25 μM, pump flow = 10 ml/min, and perfusate BSA concentration was 0.5%. *Panel B:* R6G tubing extraction ratio (ER) as a function of sampling time. R6G reservoir concentration was 0.25 μM, pump flow = 10 ml/min, tubing volume = 4 ml, and perfusate BSA concentration was 0.5%. Values are mean ± SE (n = 7, 3 for panels A and B, respectively).

3.4 Lung venous effluent R6G concentrations during the three phases of Protocol 2:

For each sample at a given sampling time, the measured intensity was determined as the average of the intensities acquired over a period of 5 seconds. For each of the three phases of the Protocol 2 experiments, the intensity of background samples was subtracted from the intensities of all subsequent samples. The slope of the standard curve for each day of experiments was then used to convert the measured intensities to R6G concentrations in the venous effluent at the time the sample was collected. The measured input R6G concentrations were slightly different from the desired 0.25 μM, which created additional variability among the results of experiments using the same experimental Protocol. To minimize this variability, the concentrations of all venous effluent samples were scaled by the ratio of 0.25 μM to the measured R6G concentration of the input sample.

Figure 3.6 shows R6G venous effluent concentrations during the three phases of Protocol 2. Results show that R6G venous effluent concentration decreased from ~ 0.13 μM during the loading phase to ~ 0.03 μM during the wash phase after switching from perfusate containing 0.25 μM R6G (loading phase) to perfusate with 0 μM R6G (wash phase). Figure 3.6 also shows that perfusing the lungs with perfusate containing FCCP (~67 μM) resulted in a rapid increase in the concentration of R6G in the venous effluent samples (uncoupling phase), consistent with the uncoupling of lung tissue mitochondria and the release of R6G that had accumulated in the mitochondria during the loading phase, driven by $\Delta\psi_m$. Thus, these data contain information about $\Delta\psi_m$, which was quantified using the computational model as described in *Data Analysis* chapter.

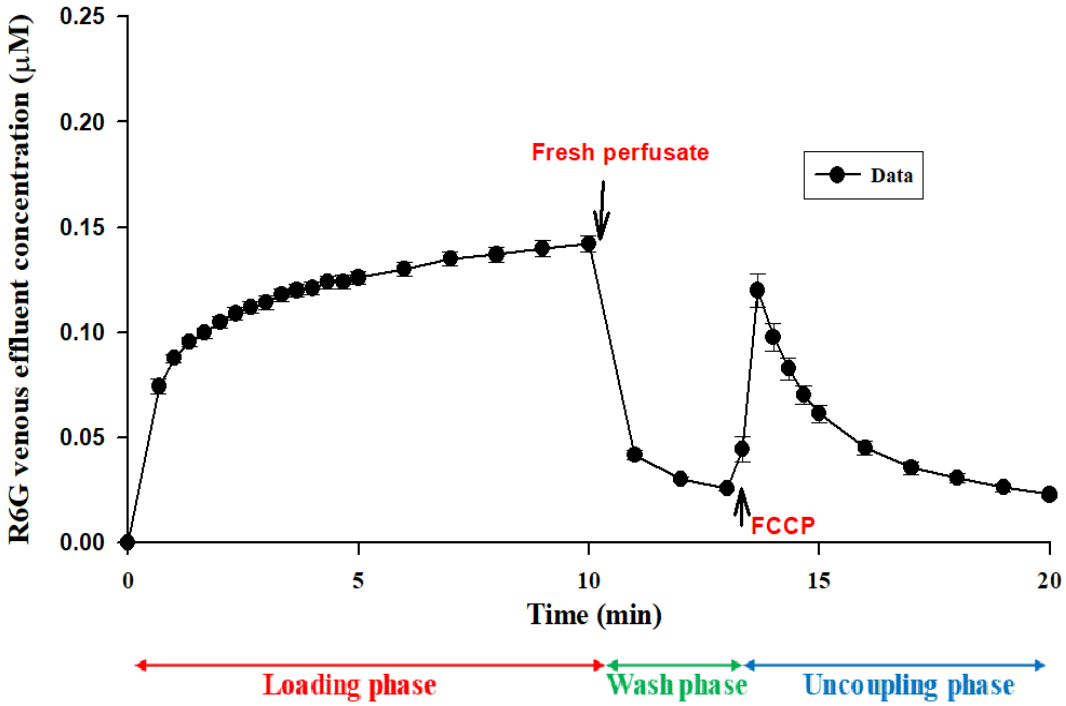

Figure 3.6: *Solid symbols:* R6G venous effluent concentrations during the loading phase, wash phase, and uncoupling phase using FCCP (67 μM). Values are mean ± SE (n = 7 for loading and wash phases, and n = 5 for uncoupling phase).

3.5 Effect of inhibitors of the multi-drug efflux pump P-glycoprotein (Pgp) on R6G lung uptake:

R6G is a known substrate for Pgp (Roerig et al., 2004). Thus, we evaluated the effect of the Pgp inhibitor verapamil on R6G venous effluent concentrations during the three phases of Protocol 2. Figure 3.7 shows the concentrations of R6G in the venous effluent following passage through lungs in which Pgp was inhibited by recirculating verapamil (0.1 mM) for 3 minutes prior to carrying out Protocol 2. In addition, verapamil (0.1 mM) was added to the perfusate during all three phases of this Protocol. The results show no significant increase in R6G uptake during the loading phase (as compared to

Figure 3.6), but a large increase in the concentration of R6G released from the lungs following the addition of FCCP to the perfusate (uncoupling phase).

Figure 3.7 also shows that adding just the vehicle (DMSO) for FCCP to the perfusate during the uncoupling phase had no effect on the concentration of R6G in the venous effluent compared to that during the wash phase.

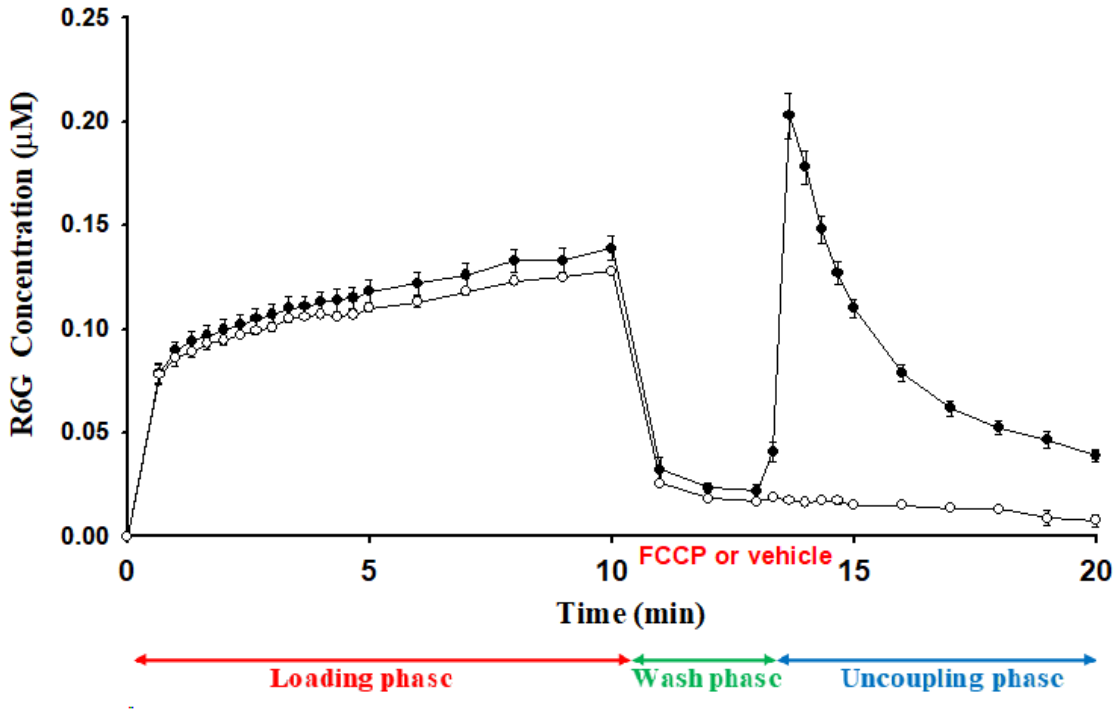

Figure 3.7: *Solid symbols:* R6G venous effluent concentration in lungs following treatment with verapamil using Protocol 2. Values are mean ± SE. n = 6, 5, 5 for loading phase, wash phase, and uncoupling phase, respectively. *Open symbols:* R6G venous effluent concentration in lungs following treatment with verapamil using Protocol 2 with DMSO (FCCP vehicle) instead of FCCP added to the perfusate during the uncoupling phase. Values are mean ± SE (n = 2).

3.6 Effects of rat exposure to hyperoxia (>95% O_2 for 48 hours) on R6G venous effluent concentrations using Protocol 2.

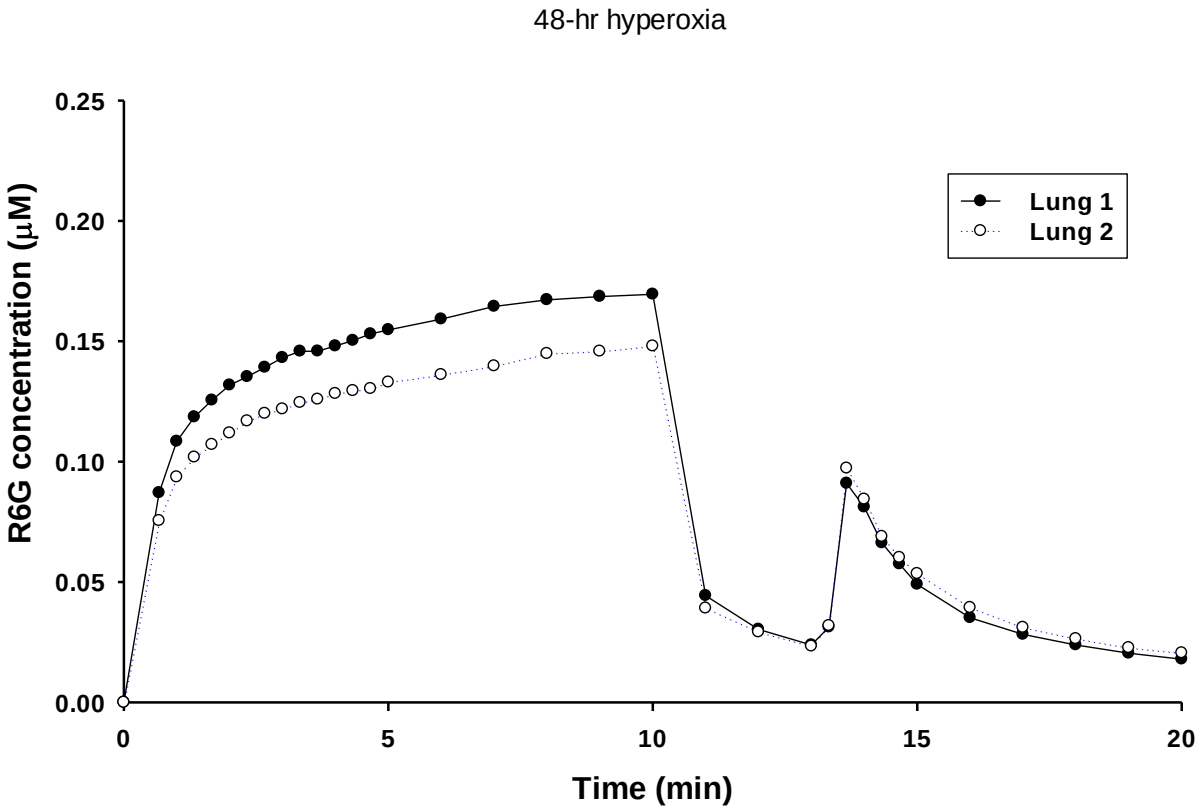

Figure 3.8: R6G venous effluent concentration using Protocol 2 in lungs from 2 rats exposed to hyperoxia for 48 hrs.

CHAPTER 4: MODEL DEVELOPMENT

4.1 Pharmacokinetic model of R6G pulmonary disposition

For mechanistic and quantitative interpretation of the R6G kinetic data, a pharmacokinetic model was developed for the pulmonary disposition of R6G. The model was used to estimate parameters descriptive of the dominant factors that determine the lung uptake and retention of R6G, including $\Delta\psi_m$.

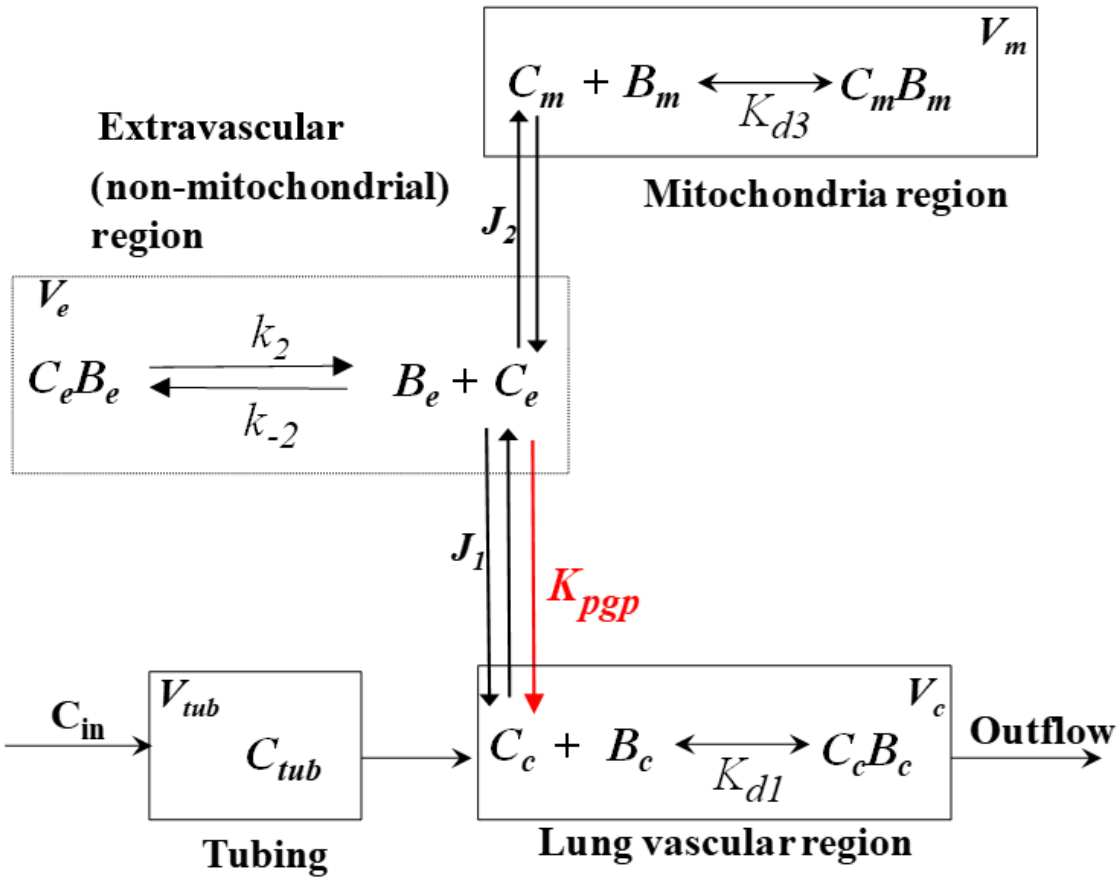

***Figure 4.1*:** Pharmacokinetic model of R6G lung uptake and retention on passage through the rat pulmonary circulation. The model consists of four regions: tubing, vascular, extravascular (non-mitochondrial), and mitochondrial with volumes V_{tub}, V_c, V_e and V_m, respectively. See below for definitions of various symbols and parameters.

The model (Figure 4.1) includes four regions, namely the tubing region, consisting of the tubing connecting the reservoir to the pulmonary artery, the lung vascular region, the extravascular (intracellular, non-mitochondrial) region, and the mitochondrial region, each with volume V_{tub}, V_c, V_e, and V_m, respectively. The model accounts for the hypothesized dominant vascular and/tissue processes that determine the lung uptake and retention of R6G on passage through the pulmonary circulation. Within the vascular region, the model accounts for the binding of R6G to BSA, which is assumed to be rapidly equilibrating with dissociation equilibrium constant K_{d1}. The model also accounts for the electrochemical gradients that drive the uptake of R6G from the vascular region to the extravascular region and from the extravascular to the mitochondrial region. R6G flux across plasma membrane (J_1) or inner mitochondrial membrane (J_2) is represented by a modified one-dimensional Goldman-Hodgkin-Katz equation (Gan et al., 2011; Huang et al., 2007). Furthermore, the model accounts for the Pgp pump which pumps R6G from the non-mitochondrial extravascular region back to the vascular region (Gan et al., 2011). The kinetic model makes no assumptions regarding the anatomical location of the Pgp protein, although it is assumed that Pgp transports R6G from the extravascular region back to the vascular region (Gan et al., 2011). At the concentration of R6G used (0.25 μM), we assume that the pump follows first-order kinetics based on the data in Figure 3.2. Within the extravascular region, the model allows for slowly equilibrating R6G interactions (Gan et al., 2011). This could represent intracellular binding or sequestration in organelles, and is assumed to be a high-capacity, high-affinity pool for R6G (Gan et al., 2011). Within the mitochondria region, the model accounts for the binding of R6G to various proteins (Scaduto et al., 1999) which is

assumed to be rapidly equilibrating with dissociation equilibrium constant K_{d3}. The inhibitor verapamil is assumed not only to inhibit (competitive inhibition) Pgp- mediated R6G efflux, but also to compete (non-competitive inhibition) with R6G for binding sites in the extravascular region (Gan et al., 2011) (see *Chapter 6*).

The rates of change in the concentrations of R6G in each of the four regions are described by the following system of differential equations, which were derived using the laws of mass balance and mass action.

4.2 Derivation of Model Equations

Glossary of terms:

$[B_e]$	Concentration of extravascular R6G binding sites (μM)
$[B_c]$ = [BSA]	Vascular BSA concentration (%BSA)
$[P_m]$	Concentration of mitochondrial R6G binding sites (μM)
$[C_{tub}]$	Free R6G concentration within the tubing region (μM)
$[C_e]$	Free R6G concentration within the extravascular region (μM)
$[C_eB_e]$	Concentration of bound R6G within the extravascular region (μM)
$[C_c]$	Free R6G concentration within the vascular region (μM)
$[C_cB_c]$	Concentration of bound R6G within the vascular region (μM)
$[\bar{C}_c]$	Total concentration of R6G within the vascular region (μM)
$[C_{in}]$	Infused R6G concentration (μM)
$[C_m]$	Free R6G concentration within the mitochondrial region (μM)
$[C_mB_m]$	Concentration of bound R6G within the mitochondrial region (μM)
Q	Flow rate (ml/min)
J_1	Dye flux across plasma membrane (nmol/(cm^2.min))
J_2	Dye flux across inner mitochondrial membrane (nmol/(cm^2.min))
k_1	Association rate constant of R6G - BSA binding in the vascular region (%BSA^{-1}.min^{-1})

k_{-1}	Dissociation rate constant of R6G-BSA binding within the vascular region (min^{-1})
k_2	Association rate constant of R6G – B_e binding in the extravascular region ($\mu M^{-1}.min^{-1}$)
k_{-2}	Dissociation rate constant of R6G – B_e binding in the extravascular region (min^{-1})
k_3	Association rate constant of R6G - B_m binding in mitochondrial region ($\mu M^{-1}.min^{-1}$)
k_{-3}	Dissociation rate constant of R6G - B_m binding in mitochondrial region (min^{-1})
$K_{d1} = k_{-1}/k_1$	Dissociation equilibrium constant for R6G - *BSA* binding in vascular region (% BSA)
$K_{d3} = k_{-3}/\bar{k}_3$	Dissociation equilibrium constant for R6G - B_m binding in the mitochondrial region
$\bar{k}_2 = k_2[B_e]$	Apparent rate constant for R6G – B_e binding in the extravascular region (min^{-1})
$\bar{k}_3 = k_3[B_m]$	Apparent rate constant for R6G - B_m binding in the mitochondrial region (min^{-1})
K_{pgp}	Rate of efflux of R6G via Pgp pump from extravascular to vascular region (ml/min)
P_1	R6G permeability across plasma membrane (cm/min)
P_2	R6G permeability across mitochondrial membrane (cm/min)
S_1	Surface area of plasma membrane (cm^2)
S_2	Surface area of mitochondrial membrane (cm^2)
V_3	Apparent volume of mitochondrial region (ml)
V_{tub}	Physical volume of tubing region (ml)
V_e	Physical volume of extravascular region (ml)
V_c	Physical volume of vascular region (ml)
V_m	Physical volume of mitochondrial region = 0.02 V_e (ml)

$\alpha = ZF/RT$	0.0374 mV^{-1} at 37 ^{o}C is a constant dependent on the universal gas constant (R), Faraday constant (F), R6G valence (Z), and absolute temperature (T).
$\Delta\psi_m$	Mitochondrial membrane potential (mV)
$\Delta\psi_p$	Plasma membrane potential (mV)

4.2.1 Tubing Region

$$\frac{d[C_{tub}]}{dt} = \frac{Q}{V_{tub}}\left([C_{in}] - [C_{tub}]\right) \tag{4.1}$$

where $[C_{in}]$ and $[C_{tub}]$ are total (free + bound) concentration of R6G in reservoir and tubing regions, respectively.

4.2.2 Vascular Region

Rates of change in the concentrations of free, $[C_c]$, and BSA-bound, $[C_cB_c]$, R6G within the vascular region:

$$V_c \frac{d[C_c]}{dt} = V_c\left(k_{-1}[C_cB_c] - k_1[C_c][B_c]\right) - S_1J_1 + K_{pgp}[C_e] + Q\left([C_{tub}]_f - [C_c]\right) \tag{4.2}$$

$$V_c \frac{d[C_cB_c]}{dt} = V_c\left(-k_{-1}[C_cB_c] + k_1[C_c][B_c]\right) + Q\left([C_{tub}]_b - [C_cB_c]\right) \tag{4.3}$$

where B_c = perfusate % BSA, and $[C_{tub}]_f$ and $[C_{tub}]_b$ are the free and BSA bound R6G concentrations in the tubing region such that,

$$[C_{tub}] = [C_{tub}]_f + [C_{tub}]_b \tag{4.4}$$

and

$$J_1 = \frac{\alpha P_1 \Delta\psi_p}{\left(e^{\alpha\Delta\psi_p} - 1\right)}\left(e^{\alpha\Delta\psi_p}[C_c] - [C_e]\right) \tag{4.5}$$

Assuming rapidly equilibrating interactions between R6G and perfusate BSA then,

$$k_{-1}[C_c B_c] = k_1[C_c][B_c] \tag{4.6}$$

$$[C_c B_c] = \frac{k_1}{k_{-1}}[C_c][B_c] = \frac{[C_c][B_c]}{K_{d1}} \tag{4.7}$$

where K_{d1} is the R6G to BSA binding equilibrium dissociation rate constant. Let

$$[\bar{C}_c] = [C_c] + [C_c B_c] = [C_c]\left(1 + \frac{[B_c]}{K_{d1}}\right) \tag{4.8}$$

then addition of equations 4.2 and 4.3 after substituting equations 4.7 and 4.8 for free and bound forms of R6G in the vascular region results in:

$$V_c \frac{d[\bar{C}_c]}{dt} = -S_1 J_1 + K_{pgp}[C_e] + Q\left([C_{tub}] - [\bar{C}_c]\right) \tag{4.9}$$

and

$$J_1 = \frac{\alpha P_1 \Delta\psi_p}{\left(e^{\alpha\Delta\psi_p} - 1\right)}\left(e^{\alpha\Delta\psi_p}\frac{[\bar{C}_c]}{\left(1 + \frac{[B_c]}{K_{d1}}\right)} - [C_e]\right) \tag{4.10}$$

4.2.3 Extravascular Region

Rates of change in the concentrations of free, $[C_e]$, and protein-bound, $[C_e B_e]$, R6G within this region:

$$V_c \frac{d[C_e]}{dt} = V_e\left(k_{-2}[C_e B_e] - \bar{k}_2[C_e]\right) - S_2 J_2 + S_1 J_1 - K_{pgp}[C_e] \tag{4.11}$$

$$V_e \frac{d[C_e B_e]}{dt} = V_e \left(-k_{-2}[C_e B_e] + \bar{k}_2[C_e]\right) \tag{4.12}$$

where $\bar{k}_2 = k_2[B_e]$ and

$$J_2 = \frac{\alpha P_2 \Delta\psi_m}{\left(e^{\alpha\Delta\psi_m} - 1\right)}\left(e^{\alpha\Delta\psi_m}[C_e] - [C_m]\right) \tag{4.13}$$

4.2.4 Mitochondrial Region

Rates of change in the concentrations of free, [C_m], and protein-bound, [$C_m B_m$], R6G within this region:

$$V_m \frac{d[C_m]}{dt} = V_m \left(k_{-3}[C_m B_m] - k_3[C_m][B_m]\right) + S_2 J_2 \tag{4.14}$$

$$V_m \frac{d[C_m B_m]}{dt} = V_m \left(-k_{-3}[C_m B_m] + k_3[C_m][B_m]\right) \tag{4.15}$$

where [B_m] = protein concentration within mitochondrial region

Assuming rapidly equilibrating interactions between R6G and B_m then:

$$k_{-3}[C_m B_m] = k_3[C_m][B_m] \tag{4.16}$$

$$[C_m B_m] = \frac{[C_m]}{K_{d3}} \tag{4.17}$$

where $K_{d3} = \dfrac{k_{-3}}{k_3[B_m]}$ is R6G and B_m binding equilibrium dissociation constant.

The addition of equations 4.14 and 4.15 after substituting equation 4.17 for [$C_m B_m$] results in

$$V_m \left(1 + \frac{1}{K_{d3}}\right) \frac{d[C_m]}{dt} = V_3 \frac{d[C_m]}{dt} = S_2 J_2 \tag{4.18}$$

where $V_3 = V_m\left(1+\frac{1}{K_{d3}}\right)$ is the apparent volume of the mitochondrial extravascular region.

4.2.5 System of governing ODE's

$$\frac{d[C_{tub}]}{dt} = \frac{Q}{V_{tub}}\left([C_{in}]-[C_{tub}]\right) \tag{4.20}$$

$$V_c\frac{d[\bar{C}_c]}{dt} = -S_1J_1 + K_{pgp}[C_e] + Q\left([C_{tub}]-[\bar{C}_c]\right) \tag{4.21}$$

$$V_e\frac{d[C_e]}{dt} = V_e\left(k_{-2}[C_eB_e]-\bar{k}_2[C_e]\right) - S_2J_2 + S_1J_1 - K_{pgp}[C_e] \tag{4.22}$$

$$V_e\frac{d[C_eB_e]}{dt} = V_e\left(-k_{-2}[C_eB_e]+\bar{k}_2[C_e]\right) \tag{4.23}$$

$$V_3\frac{d[C_m]}{dt} = S_2J_2 \tag{4.24}$$

where

$$J_1 = \frac{\alpha P_1\Delta\psi_p}{\left(e^{\alpha\Delta\psi_p}-1\right)}\left(e^{\alpha\Delta\psi_p}\frac{[\bar{C}_c]}{\left(1+\frac{[B_c]}{K_{d1}}\right)}-[C_e]\right) \tag{4.25}$$

$$J_2 = \frac{\alpha P_2\Delta\psi_m}{\left(e^{\alpha\Delta\psi_m}-1\right)}\left(e^{\alpha\Delta\psi_m}[C_e]-[C_m]\right) \tag{4.26}$$

$[C_{tub}](t)$ and $[\bar{C}_c](t)$ are R6G total (free + bound) concentrations (μM) at time *t* in the tubing and vascular regions, respectively; $[C_e](t)$ and $[C_m](t)$ are R6G free concentrations in extravascular and mitochondrial regions at time *t*, respectively;

$[C_eB_e](t)$ is R6G bound concentration in the extravascular region at time t; $[C_{in}]$ is the R6G concentration in the reservoir; $[B_c]$ is % BSA in perfusate; $[B_m]$ is the concentration of R6G binding sites within the mitochondrial region; Q (ml/min) is pump flow; P_1S_1 (ml/min) and P_2S_2 (ml/min) are products of R6G permeability (P) across plasma and mitochondrial membranes, respectively, and the surface area (S) of these membranes; K_{pgp} is Pgp-mediated dye efflux rate (ml/min); $K_{d1} = \frac{k_{-1}}{k_1}$ (%BSA) is the dissociation equilibrium constant for R6G-BSA binding in the vascular region; $K_{d3} = \frac{k_{-3}}{k_3[B_m]}$ is the dissociation equilibrium constant for R6G - B_m binding within the mitochondria region; $V_3 = V_m\left(1+\frac{1}{K_{d3}}\right)$ is the apparent volume (ml) of the mitochondrial region; k_i and k_{-i} are R6G and protein/binding sites association and dissociation rate constants, respectively, with B_c (i =1) and B_m (i = 3), respectively; $\bar{k}_2 = k_2[B_e]$ (min^{-1}) and k_{-2} (min^{-1}) are rate constants for R6G binding and unbinding with binding sites B_e within V_e, respectively, and $[B_e]$ is the concentration of those binding sites; $\alpha = ZF/RT$ = 0.0374 mV^{-1} at 37 ^{o}C is a constant dependent on gas constant, Faraday constant, R6G valence, and absolute temperature; $\Delta\psi_m$ and $\Delta\psi_p$ are mitochondrial and plasma membrane potential (mV), respectively.

***Table 4.1*:** Model Parameters

Symbol	Description	Units
$K_{d1} = k_{-1}/k_1$	Dissociation equilibrium constant for R6G-BSA binding in the vascular region	%BSA
$\bar{k}_2$	Apparent rate constant for R6G-B_c binding within the cytoplasm region	min^{-1}
k_{-2}	Dissociation rate constant of R6G-B_c binding within the cytoplasm region	min^{-1}
K_{d3}	Dissociation equilibrium constant for R6G-B_m binding within the mitochondria region	
K_{pgp}	Rate of efflux of R6G via Pgp pump from cytoplasm to the vascular region	ml/min
P_1S_1	R6G permeability-surface area product across the plasma membrane	ml/min
P_2S_2	R6G permeability-surface area product across the mitochondrial membrane	ml/min
$\Delta\psi_m$	Mitochondrial membrane potential	mV

The PBPK model R6G extraction ratio (ER) at a given time t, a measure of the fraction of the input that is extracted on passage through the lungs, is given by the following equation

$$ER = 1 - \frac{[\overline{C_e}]}{[C_{in}]} \tag{4.27}$$

4.3 Estimation of Model Parameters

To reduce the number of unknown model parameters, the lung vascular volume (V_c) was set at 0.85 ml (Audi et al., 2003) and the lung extravascular volume (V_e) was set at 1.0 ml based on lung tissue water volume estimated from lung wet weight and wet-to-dry weight ratio (Audi et al., 2003). To break the correlation between V_m and $\Delta\psi_m$, the ratio V_m/V_e was set to 0.02, consistent with a lower bound measured for this ratio in rat pulmonary endothelium (Gan et al., 2011). To break the correlation between P_1S_1 and $\Delta\psi_p$, the value

of $\Delta\psi_p$ was set to that (-43 mV) estimated by Gan et al. in cultured pulmonary arterial endothelial cells (Gan et al., 2011). Furthermore, we assumed complete dissipation of $\Delta\psi_m$ in the presence of FCCP at the concentration used (67 μM) (Zhao et al., 2013; Huang et al., 2018), and complete inhibition of Pgp in the presence of verapamil at the concentration used (100 μM) (Roerig et al., 2004). Then, $\Delta\psi_m$, K_{pgp}, $K_{d1,}$ $K_{d3,}$ $\bar{k}_2$, k_{-2}, P_1S_1, and P_2S_2 are the unknown model parameters (Table 4.1). The model-governing differential equations were solved numerically using the MATLAB (MathWorks) function "*ode45*," which is based on an explicit Runge-Kutta formula. The equations were solved with the following initial (t = 0) conditions: $[\bar{C}_c](0) = [C_e](0) = [C_m](0) = 0$ and $[C_{tub}](0) = [C_{in}]$ for Protocol 1 and loading phase of Protocol 2, and $[C_{tub}](0) = 0$ for wash and uncoupling phases of Protocol 2.

CHAPTER 5: DATA ANALYSIS

5.1 Experimental Data Analysis

Data analysis was performed in *Excel and Matlab* using text files exported from PTI's Felix software.

5.1.1 Standard Curve

For each standard R6G concentration, the R6G fluorescent intensity was determined from the average intensity measurements acquired over a period of 5 seconds. The average intensity of the sample with no R6G added was considered background, and this intensity was subtracted from the intensities of samples with different R6G concentrations. The resulting intensities were then plotted against the known R6G concentrations added to each standard sample. As shown in Figure 5.1, linear regression was then used to estimate the slope of the standard curve which was then used to convert R6G intensity in each lung to R6G concentration.

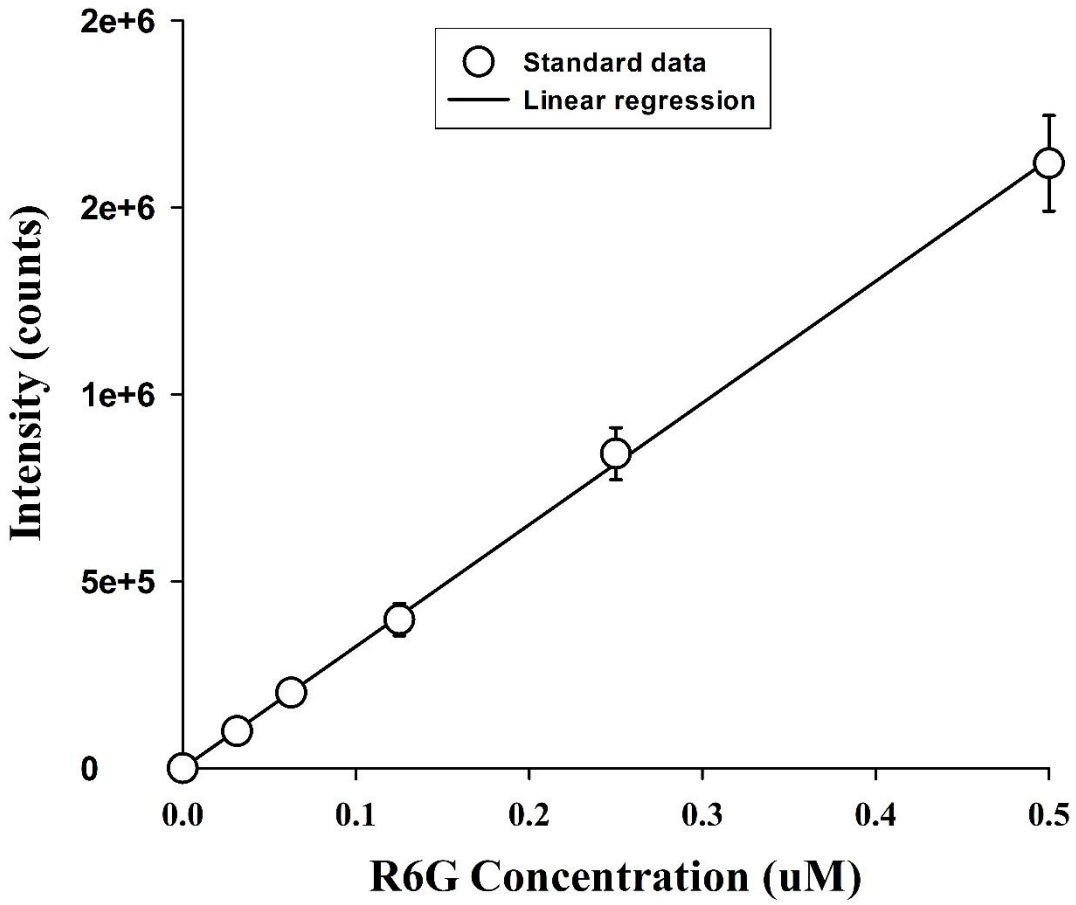

Figure 5.1: Representative standard curve for R6G. This is done to have a way of converting the recorded emission values from experimentation to concentration values. This procedure was performed for every experimental data set. Values are mean ± SE (n = 7).

5.2 Fit of PBPK model to data

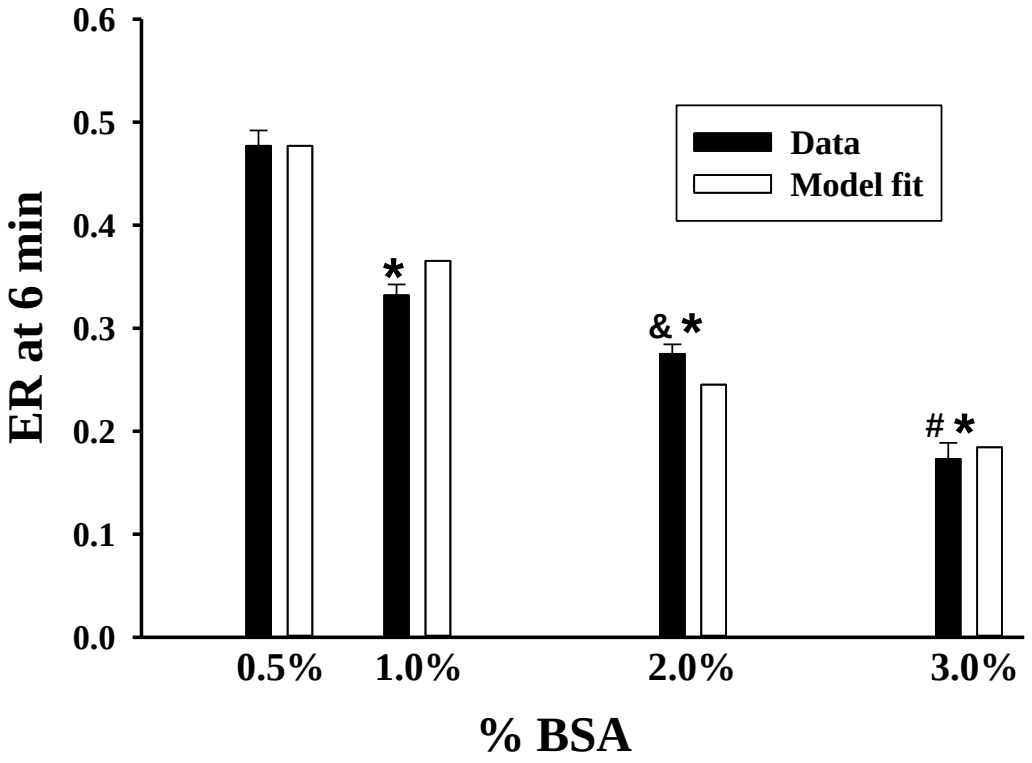

Figure 5.2: R6G lung extraction ratio (ER, solid bars) after 6 min of perfusion (single pass) as a function of perfusate %BSA. Pump flow = 10 ml/min. Values are mean ± SE (n = 10, 3, 3 and 4 for perfusate BSA of 0.5, 1.0, 2.0, and 3.0%, respectively. Open bars are model fit values. [*]significantly different from 0.5% BSA ($P < 0.05$, unpaired t-test), [&]significantly different from 1.0% ($P < 0.05$), and [#] significantly different from 2.0% ($P < 0.05$).

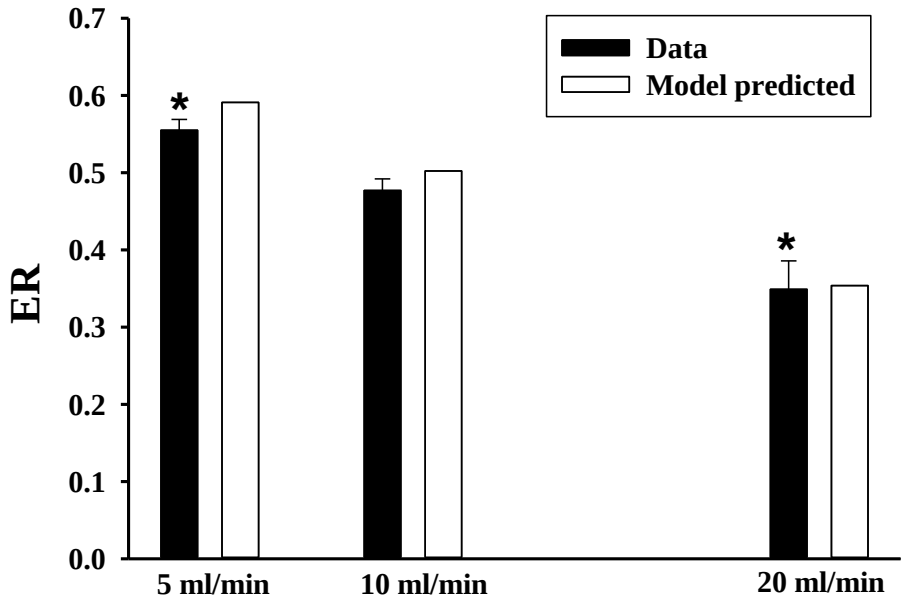

Figure 5.3: R6G lung extraction ratio (ER, solid bars) after 12 min, 6 min, and 3 min of perfusion (single pass) with pump flow set at 5, 10, or 20 ml/min, respectively. Values are mean ± SE (n = 4, 10, and 6 for flow of 5, 10, and 20 ml/min, respectively. Open bars are model prediction. *significantly different from ER at flow of 10 ml/min ($P < 0.05$, unpaired *t*-test).

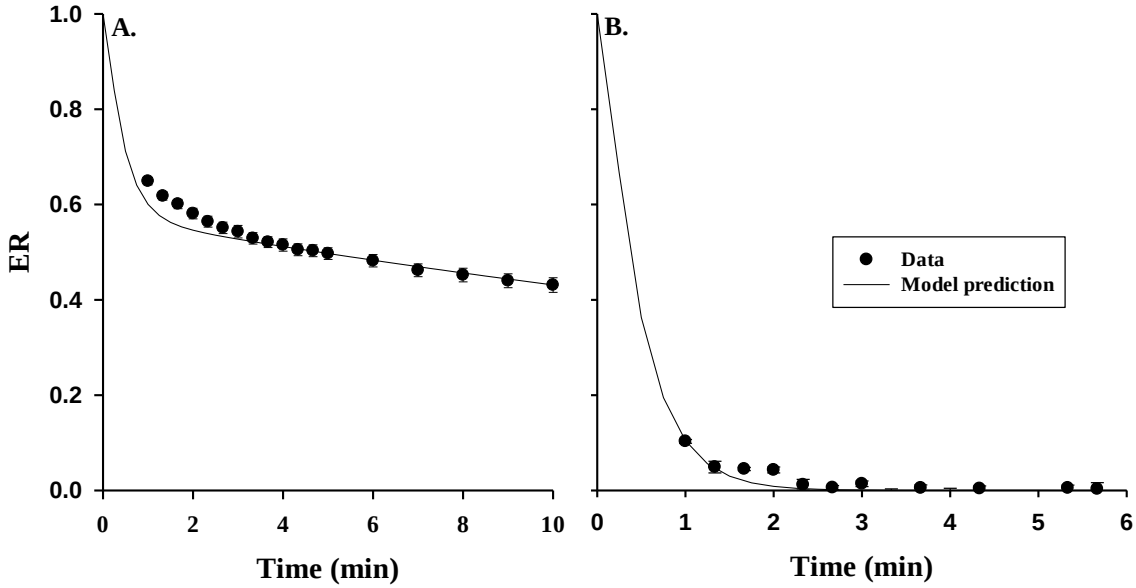

Figure 5.4: *Panel A:* R6G lung extraction ratio (ER) as a function of sampling time on passage through the pulmonary circulation. R6G reservoir concentration was 0.25 μM, pump flow = 10 ml/min, and perfusate BSA concentration was 0.5%. *Panel B:* R6G tubing extraction ratio (ER) as a function of sampling time. R6G reservoir concentration was 0.25 μM, pump flow = 10 ml/min, tubing volume = 4 ml, and perfusate BSA concentration was 0.5%. Solid line is model prediction. Values are mean ± SE (n = 7, 3 for panels A and B, respectively).

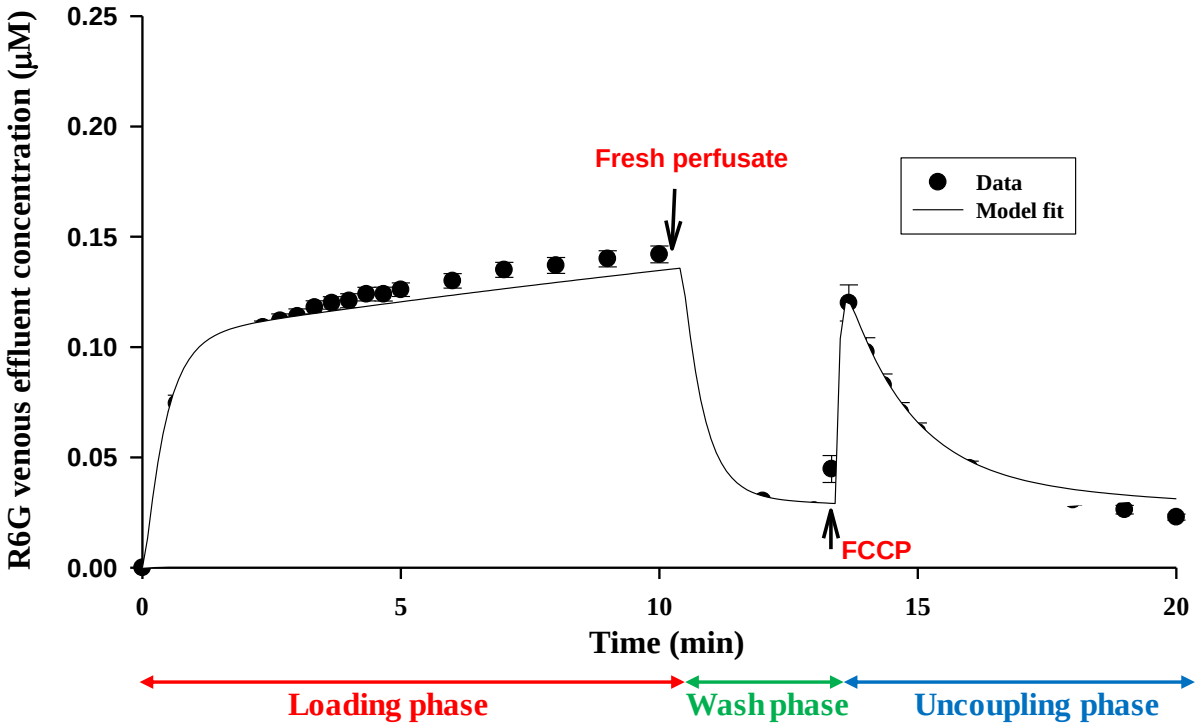

Figure 5.5: *Solid symbols:* R6G venous effluent concentrations during the loading phase, wash phase, and uncoupling phase using FCCP (67 μM). Values are mean ± SE (n = 7 for loading and wash phases, and n = 5 for uncoupling phase). Solid line is model fit to data.

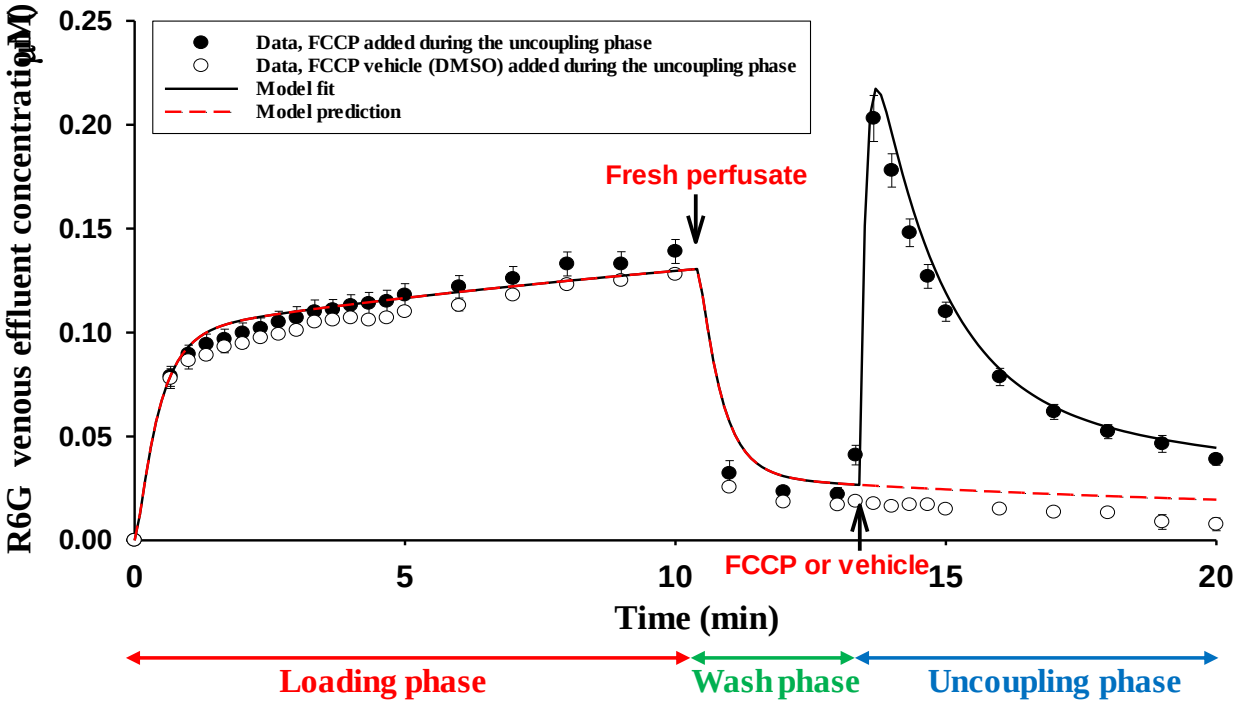

Figure 5.6: *Solid symbols:* R6G venous effluent concentration in lungs following treatment with verapamil using Protocol 2. Values are mean ± SE. n = 6, 5, 5 for loading phase, wash phase, and uncoupling phase, respectively. *Open symbols:* R6G venous effluent concentration in lungs following treatment with verapamil using Protocol 2 with DMSO (FCCP vehicle) instead of FCCP added to the perfusate during the uncoupling phase. Values are mean ± SE (n = 2). Solid line is model fit to mean of the solid symbols. Dashed line is model prediction of the open symbols.

For data from *Protocol* 1, the results (Figure 5.3) are expressed as the extraction ratio (ER) as a function of flow rate. The flow rate R6G extraction data in Figure 5.3 contains information about PS_1. Whereas the R6G extraction data in Figure 5.6 contain information about k_{pgp}. All the data also contain information about k_{d2}, k_{d3}, and $\Delta\Psi_m$.

To characterize the pulmonary pharmacokinetics of R6G, information about its permeability across the plasma membrane is needed. This information can be obtained by evaluating the impact of changing perfusate flow rate (and hence pulmonary transit time) on the lung ER of R6G. A small change in ER with flow would suggest that cell membrane permeability for R6G is relatively high, whereas a large change would be

consistent with a significant barrier for the uptake of R6G on passage through the pulmonary circulation.

5.3 Estimation of model parameters

The first step in the procedure to estimate the unknown parameters was to fit the mean kinetic data of Protocol 2 in the absence of verapamil (Figure 5.5) and the ER values at the four different perfusate %BSA (Figure 5.2) simultaneously. The objective was to obtain an estimate of K_{d1} for R6G binding with perfusate BSA, and initial estimates of the other unknown parameters (Table 4.1). The model fitting was done in MATLAB® using the *lsqcurvefit* function to implement the trust-region-reflective algorithm, an iterative optimization algorithm that readily incorporates bounds on the values of the parameters.

The estimated values of model parameters that best fit the data along with the model fits are shown in Table 5.1 and Figures 5.2 and 5.5, respectively. Based on the estimated values of K_{d1} (0.32 %BSA, Table 2), R6G is ~61% bound to BSA in perfusate that includes 0.5% BSA.

Table 5.1: Values of model parameters estimated by simultaneously fitting the data in Figures 5.2 and 5.5.

P_1S_1 (ml/min)	P_2S_2 (ml/min)	K_{pgp} (ml/min)	$\bar{k}_2$ (ml/min)	k_{-2} (min^{-1})	K_{d3}	$\Delta\psi_m$ (mV)	K_{d1} (%BSA)
45.40	0.71	6.19	11.13	0.1223	0.0327	- 118.21	0.32

Next, K_{d1} was fixed at the value in Table 5.1, and the other model parameters were estimated from the kinetic data from individual Protocol 2 experiments without or with verapamil added to the perfusate (Figures 5.5 and 5.6). In the presence of verapamil,

the value of K_{pgp} was set to zero. The estimated values of the model parameters are shown in Table 5.2 and Figures 5.5 and 5.6. The ability of the model to fit data from individual experiments is exemplified in Figure 5.7 for Protocol 2 with and without verapamil added to the perfusate. The estimated values of the model parameters show that verapamil not only inhibited Pgp, but also had a significant effect on the binding of R6G in the extravascular region (see *Chapter 6*).

Table 5.2: Values of model parameters estimated by fitting model to kinetic Protocol 2 data from individual lungs in absence or presence of verapamil in the perfusate

	P_1S_1 (ml/min)	P_2S_2 (ml/min)	K_{pgp} (ml/min)	$\bar{k}_2$ (ml/min)	k_{-2} (min^{-1})	K_{d3}	$\Delta\psi_m$ (mV)
R6G	48.81 ± 0.66	0.82 ± 0.04	8.98 ± 1.55	12.67 ± 0.58	0.111 ± 0.005	0.023 ± 0.002	- 123.8 ± 0.8
R6G + verapamil	46.69 ± 0.32*	1.12 ± 0.16	0	7.00 ± 0.51*	0.172 ± 0.022*	0.016 ±0.002*	- 130.6 ± 5.2

Values are mean ± SE (n = 6 and 5 without and with verapamil, respectively). *different from without verapamil (*t*-test, $P < 0.05$). K_{d1} (%BSA) was fixed at the value in Table 5.1.

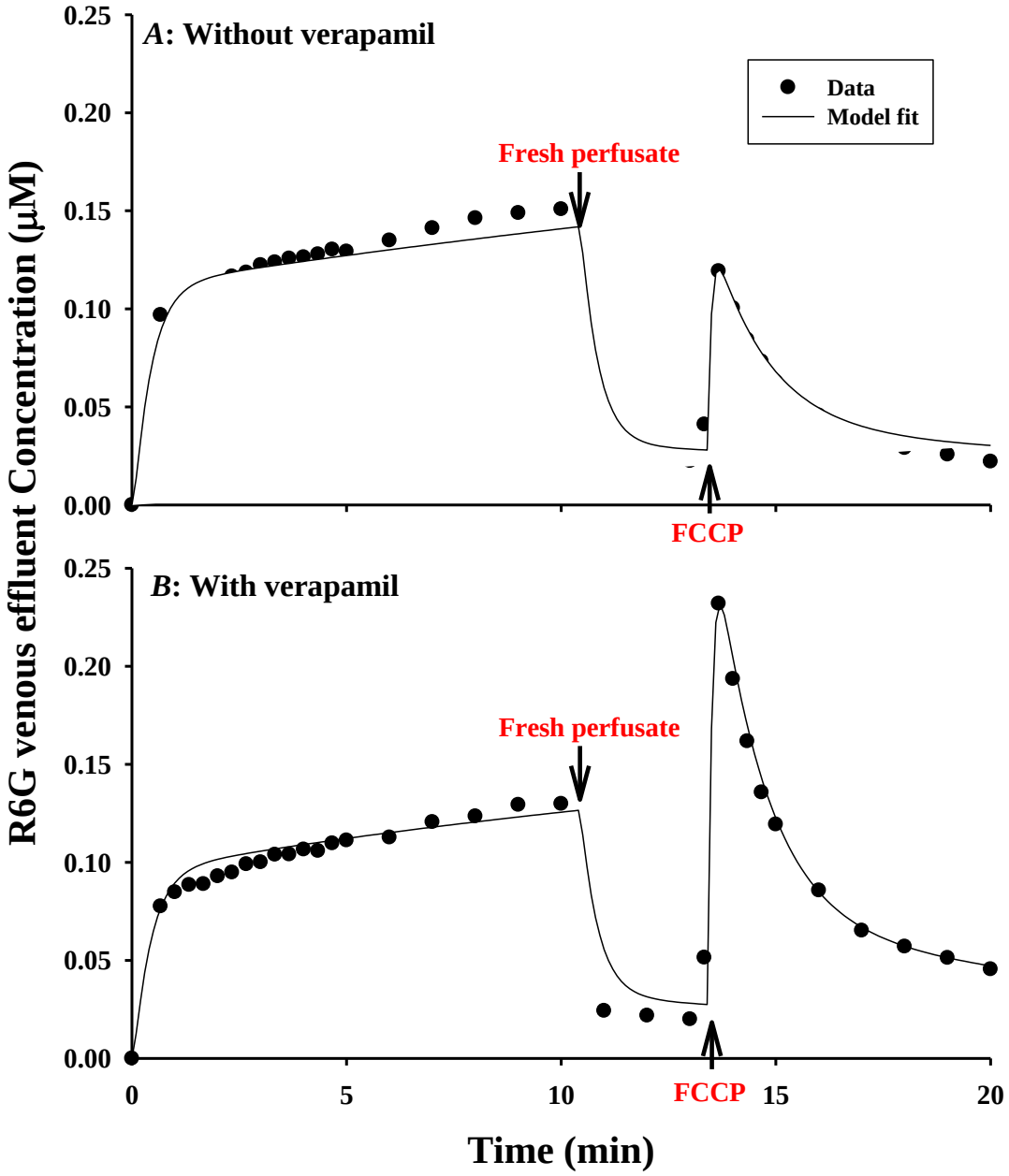

Figure 5.7: *Solid symbols:* Representative R6G lung venous effluent concentration vs. time data using Protocol 2 without (Panel A.) or with (Panel B.) lung treatment with verapamil. *Solid line* is model fit.

5.4 Model Validation

To validate the model, we assessed its ability to predict experimental data that were not used for model development, including estimation of the values of the unknown model parameters. To that end, we evaluated the ability of the model to predict the experimental data in Figure 5.5 at the different pump flows. The kinetic model and the mean of the estimated best fit values of model parameters without verapamil (Table 5.2) were evaluated by predicting the effect of pump flow on R6G ER at flows of 5 ml/min and 20 ml/min (Figure 5.3). The results in Figure 5.3 show that the predicted ER values are close to the measured values, providing support for the model and the estimated values of the model parameters (Table 5.2).

5.5 Measures of estimability of the model parameters

The estimability of the model parameters from the Protocol 2 kinetic data in Figures 5.5 and 5.6 was evaluated using a Monte Carlo approach and sensitivity analysis (Dutta et al., 1997; Bassingthwaighte et al., 1984). For the Monte Carlo approach, the model was fit to the Protocol 2 mean data without (Figure 5.5) or with (Figure 5.6) verapamil and was repeated 100 times with different initial values for the model parameters. The initial values were determined as the mean of the estimated best fit values given in Table 5.2 (without or with verapamil) + a uniformly distributed random value within ± 30% of this mean. The resulting estimated values from the 100 fits are shown in Table 5.3. The results show smaller standard deviation (SD) for $\Delta\Psi_m$ from data with verapamil (Figure 5.6) compared to no verapamil (Figure 5.5) added to the perfusate (see *Chapter 6*).

Table 5.3: Estimated values of model parameters (Monte Carlo approach): 100 different fits to mean data in the absence or presence of verapamil with the initial values of model parameters equal to the mean values of the fits to individual experiments (Table 5.2) ± a uniformly-distributed random value within ± 30% of this mean error

	P_1S_1 (ml/min)	P_2S_2 (ml/min)	K_{pgp} (ml/min)	$\bar{k}_2$ (ml/min)	k_{-2} (min^{-1})	K_{d3}	$\Delta\psi_m$ (mV)
R6G	49.37 ± 7.27	0.769 ± 0.156	13.504 ± 4.768	14.78 ± 2.37	0.118 ± 0.013	0.028 ± 0.010	- 138.82 ± 20.67
R6G + Verapamil	49.19 ± 9.11	1.178 ± 0.326	0	7.21 ± 0.63	0.168 ± 0.019	0.015 ± 0.003	- 128.09 ± 13.86

Values are mean ± SD

The estimability of the model parameters from the Protocol 2 kinetic data in Figures 5.5 and 5.6 was also evaluated using sensitivity analysis. Parameters values were set to the mean of the best fit values estimated from the individual experiments (Table 5.2). Figure 5.8 shows the corresponding sensitivity functions that represent the normalized change in the model-fit for a 1% change in the value of each free parameter. The results show similarly shaped sensitivity functions for P_2S_2 and $\Delta\psi_m$ during the loading phase of Protocol 2, but different shapes during the wash and uncoupling phases. For the wash phase, the sensitivity function for P_2S_2 is close to zero, but different from zero for $\Delta\psi_m$. This relative similarity between the sensitivity functions of P_2S_2 and $\Delta\psi_m$ during the loading and uncoupling phases may reflect a correlation between those two parameters and is consistent with the relatively large SD for both parameters in Table 5.3. See *Chapter 6* for potential approaches to reduce this correlation.

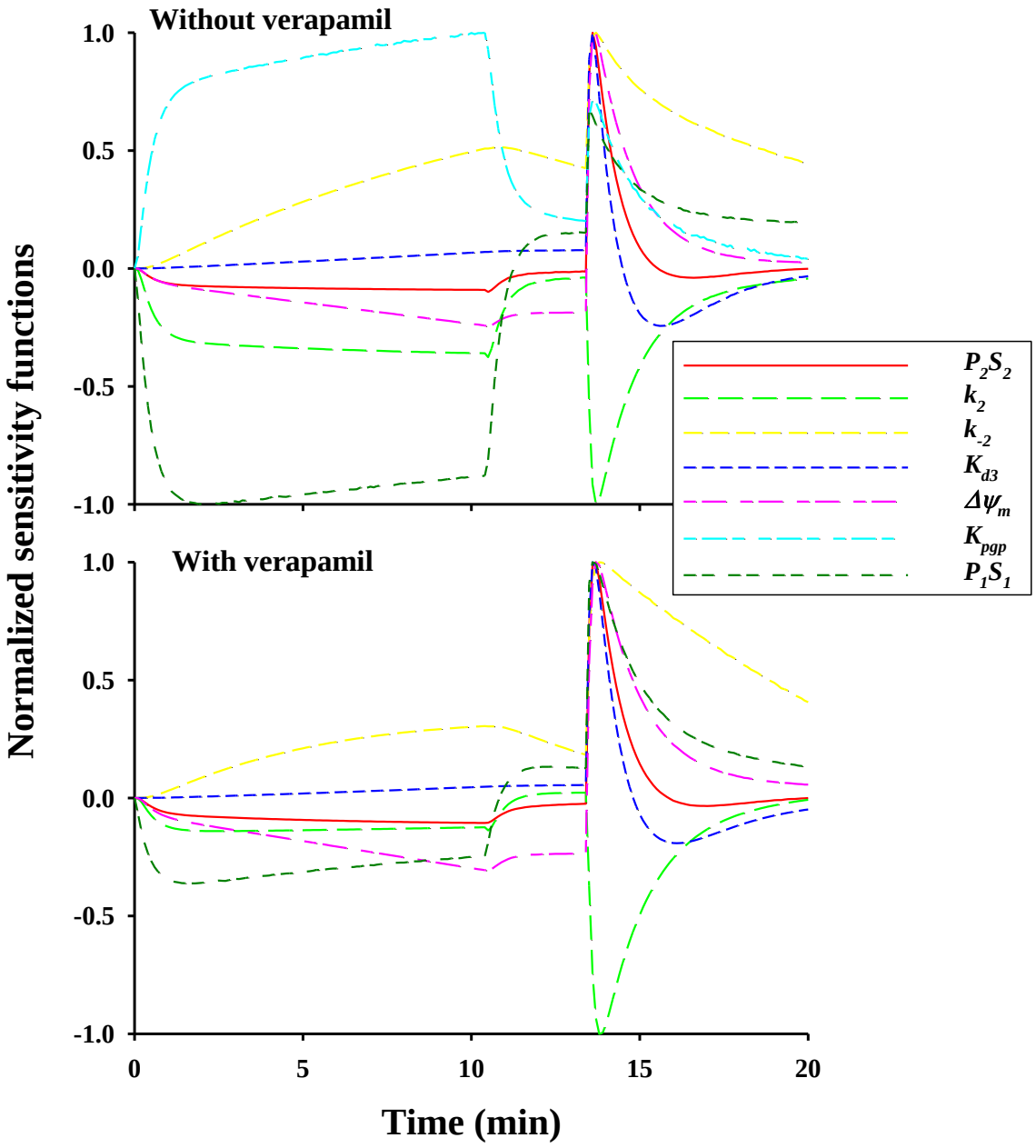

Figure 5.8: Model parameter sensitivity functions using Protocol 2 without (*top panel*) or with (*bottom panel*) verapamil. The sensitivity functions show the change in the model solution given a 1% increase in the value of a given model parameter. Each plot is normalized to its maximum value.

5.6 Sensitivity of Protocol 2 experiments to depolarization and hyperpolarization of $\Delta\psi_m$:

To assess to ability of Protocol 2, without and with verapamil added to the perfusate, to detect a change in $\Delta\psi_m$, model simulations (Figure 5.8) were generated using the mean values of the estimated parameters in Table 5.2. The value of $\Delta\psi_m$ *was* decreased (depolarization) or increased (hyperpolarization) with the values of the other model parameters set to the mean values in Table 5.2. Results show that the uncoupled phase is highly sensitive to a change in $\Delta\psi_m$, and that the sensitivity to $\Delta\psi_m$ depolarization is larger in the presence of verapamil than in its absence.

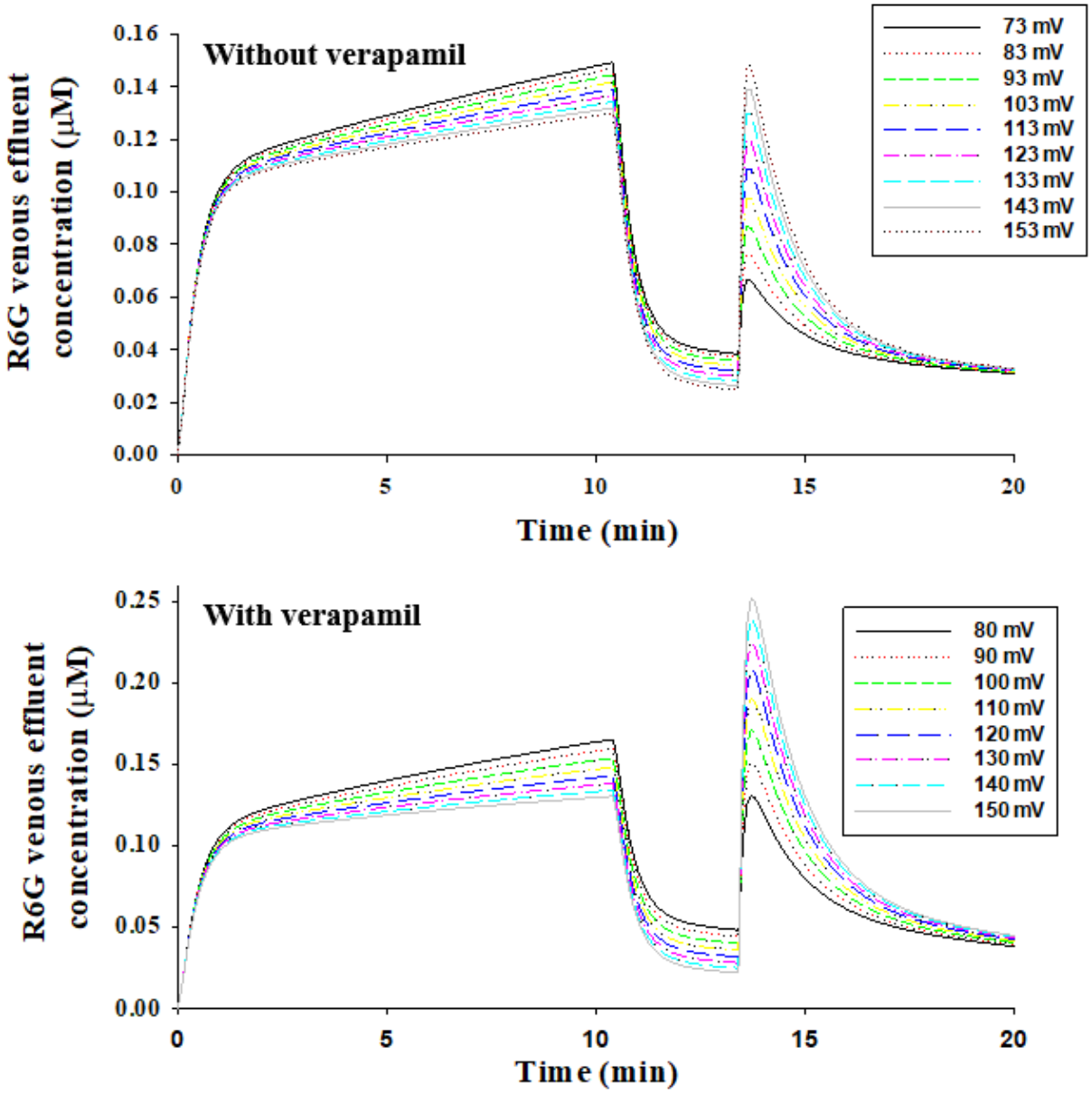

Figure 5.9: Model predictions of the sensitivity of lung R6G venous effluent concentrations using Protocol 2 to depolarization or repolarization of mitochondrial membrane potential without (*top panel*) or with (*bottom panel*) verapamil. Mean values of model parameters in Table 5.2 were used to generate these simulations.

CHAPTER 6: DISCUSSION AND CONCLUSIONS

6.1 Overview and Interpretation of Results:

This thesis describes a fluorometric experimental and computational approach for evaluating lung tissue $\Delta\psi_m$ in isolated perfused rat lungs using the lipophilic cationic dye R6G. The approach is based on changes in the lung R6G inlet-outlet perfusate concentrations before and after uncoupling the lung tissue mitochondria. A pharmacokinetic model was developed and used for quantitative interpretation of the resulting kinetic data and for estimating parameters that describe the dominant processes that determine the disposition of R6G on passage through the rat lungs, including $\Delta\psi_m$. The model and estimated parameters were validated by determining their ability to reasonably predict the effect of pump flow on the extraction ratio of R6G on passage through the lungs over a wide range of flows. The estimated value of $\Delta\psi_m$ is consistent with that estimated from cultured pulmonary arterial endothelial cells (Gan et al., 2011).

The lung is a complex organ with multiple vascular and tissue processes determining the pulmonary disposition of R6G. To overcome this complexity, we used inhibitors and a variety of perfusion conditions to target the dominant processes that are hypothesized to determine the pulmonary disposition of R6G. This provided us with discriminating information about those processes. In addition, we used a computational model to interpret the data. Computational modeling provides a mechanistic and quantitative framework that accounts for those processes and allows us to estimate parameters descriptive of those processes, including $\Delta\psi_m$ (Gan et al., 2011; Roerig et al., 2004; Gan et al., 2011). The pharmacokinetic model developed in the present study is an

extension of the model developed by Roerig et al. for the disposition of R6G in rabbit lungs to evaluate the lung activity of Pgp (Roerig et al., 2004). Unlike the model developed in the present study, their model did not account for the role of $\Delta\psi_m$ and $\Delta\psi_p$ in the lung uptake and retention of R6G. For the study by Roerig et al., the objective was to evaluates the kinetics of the Pgp pump in isolated perfused rabbit lungs.

Generally speaking, a single experimental condition or data set of the type presented here does not contain sufficient information to estimate the parameters of the pharmacokinetic model (Gan et al., 2011; Roerig et al., 2004; Gan et al., 2011). Instead, a diverse set of experimental conditions was needed to provide sufficiently discriminating information about the dominant processes that determine R6G uptake and retention in the lung. This approach is needed to break the correlation between some of the model parameters that describe these processes. Both measures of estimability of model parameters from the kinetic data using Protocol 2 without or with verapamil (Figure 5.8 and Table 5.3) suggest a relatively high correlation between $\Delta\psi_m$ and P_2S_2 during the loading and uncoupling phases, but not during the wash phase. This observation is consistent with the relatively high standard deviation of the estimated values of $\Delta\psi_m$ and P_2S_2 using the Monte Carlo approach (Table 5.3). One approach to reduce this correlation would be to extend the duration of the wash phase or to include additional experimental data, such as Protocol 2 under a different flow.

Previous studies using cationic dyes to probe $\Delta\psi_m$ have predominately been carried out in reduced systems, including isolated mitochondria and cultured cells (Gan et al., 2011; Audi et al., 2017; Perry et al., 2011; Aiuchi et al., 1982; Johnson et al., 1981; Scaduto et al., 1999; Mandala et al., 1999; Huang et al., 2007; Chen et al., 1988; Agard et

al., 2009; Davis et al., 1985; Baracca et al., 2003). Gan at al. developed an approach for quantifying $\Delta\psi_m$ and plasma membrane potential in cultured pulmonary endothelial cells based on the disposition of rhodamine dyes in the medium surrounding the cultured cells (Gan et al., 2011). The experimental and computational approach described in the present study is an extension of their approach to isolated perfused rat lungs. The estimated value of $\Delta\psi_m$ in the present study (-124 ± 1 (SE) mV and -131 ± 5 mV without and with verapamil, respectively) is consistent with that estimated by Gan et al. in cultured pulmonary endothelial cells (-130 ± 3 (SE) mV and -133 ± 1 mV) using rhodamine 123 and TMRE, respectively) (Gan et al., 2011).

For the present study, R6G was chosen since its uptake is rapid enough to accumulate within the lung tissue on a single pass through the pulmonary circulation (Roerig et al., 2004). This is in part due to its relatively high octanol/water partition coefficient compared to that of other rhodamine dyes such as R123 (Mottram et al., 2012). Our data are consistent with the large (relative to flow) estimated values of P_IS_I for R6G (Table 5.2) and its high permeability in cell membranes in a wide range of cells, including endothelial cells (Mandala et al., 1999; Loetchutinat et al., 2003). Furthermore, under the experimental conditions used in the present study (10 ml/min flow, 0.5% BSA, and 0.25 μM input concentration), R6G ER is ~ 0.5 (Figure 5.4A), which is midway within the 0 to 1 dynamic range for ER, and hence optimal for detection of depolarization or repolarization of $\Delta\psi_m$.

Previous studies evaluated the effect of R6G on mitochondrial functions (Williams et al., 1999; Gear et al., 1974). Using isolated rat liver mitochondria, ARL Gear showed that R6G at concentration > 1 μM can have a significant inhibitory effect

($K_i \sim 3$ μM) on mitochondrial membrane potential and ATP-supported calcium accumulation. Using cultured human skin fibroblasts, Williams et al. showed that cells cultured (3-8 days) in R6G-containing culture medium experienced poor growth for R6G concentrations as low as 1.2 μM. In addition, this prolonged cell treatment with R6G significantly decreased the number of intact mitochondrial and electron transport chain enzyme activities. For the present study, the concentration of R6G in the lung perfusate was 0.25 μM, well below the 1 μM at which toxic effects on mitochondrial functions were observed, and the lungs were perfused with this concentration for 10 minutes. In addition, the binding or R6G to BSA in perfusate decreased the concentration of perfusate R6G available for cellular uptake to closer to 0.125 μM. Thus, for the present study the experimental conditions, including the chosen R6G concentration, minimized the potential effects of R6G on mitochondrial functions.

Comparison of the data in Figure 5.7 shows that lung treatment with verapamil had no effect on the uptake and retention of R6G during the loading phase, although it had a significant effect during the uncoupling phase of Protocol 2. Model simulations (not shown) revealed that this increase cannot be explained by just the inhibition of the Pgp pump, and in fact the R6G efflux concentration was predicted to decrease during the uncoupling phase. The estimated values of the model parameters (Table 5.2) suggest that verapamil not only inhibited the Pgp pump, but also competed with R6G for the slowly equilibrating binding sites in the extravascular region. This effect countered the increase in lung uptake of R6G due to the inhibition of the Pgp pump, and allowed the R6G released from the mitochondrial region into the extravascular region during the uncoupling phase to diffuse quickly into the vascular region driven by the increase in the

concentration gradient of free R6G across the plasma membrane (Roerig et al., 2004; Cho et al., 2000).

Unlike the results of the present study, Roerig et al. showed a significant increase in R6G lung uptake in the presence of verapamil compared to in its absence in isolated perfused rabbit lungs (Roerig et al., 2004). This could be due to the relatively large rate of Pgp-mediated R6G efflux compared to that for cytosolic R6G binding in rabbit lungs (1.44 min^{-1} vs. 0.23 min^{-1}) (Roerig et al., 2004). For rat lungs, the rate of Pgp-mediated R6G efflux was comparable to that for cytosolic R6G binding (13.5 min^{-1} vs. 14.8 min^{-1}) (Table 5.2). In addition, for the rabbit lungs, the rate of Pgp-mediated R6G efflux is an order of magnitude larger than the rate of R6G efflux by diffusion across the cell membrane, whereas in the rat lungs P_1S_1 was much larger than the rate of Pgp-mediated efflux (Table 5.2).

One question that could be addressed using the proposed computational model is the sensitivity of Protocol 2 to a change in $\Delta\psi_m$ in the presence or absence of verapamil. Model simulations (Figure 5.8) show that Protocol 2 in the presence of verapamil has a higher sensitivity to depolarization of $\Delta\psi_m$ than in the absence of verapamil. This is in part due to a decrease in the competition between cytoplasm binding and mitochondria for free R6G in the cytoplasm. This and the reduction in the number of unknown parameters for Protocol 2 in the presence of verapamil suggest that Protocol 2 in the presence of verapamil is preferable for evaluating $\Delta\psi_m$ in isolated perfused lungs for conditions expected to cause dissipation of $\Delta\psi_m$.

Scaduto et al. attempted to probe $\Delta\psi_m$ in isolated perfused rat hearts by monitoring the surface emission fluorescence of the cationic rhodamine dye tetramethyl

rhodamine methyl ester perchlorate (TMRM) following its addition to perfusate that was recirculated through the heart (Scaduto et al., 1999). However, the results with a mitochondrial uncoupler and substrate-free perfusate were difficult to interpret in part because of alteration in the fluorescent properties of TMRM in heart tissue due to accumulation of TMRM in both mitochondria and cytosol (Scaduto et al., 1999). The approach described in the present study overcame this limitation by 1) determining the lung uptake of R6G from the lung inlet and outlet R6G perfusate concentrations on passage through the pulmonary circulation instead of from lung surface measurements, and 2) by using computational modeling for quantitative interpretation of the resulting kinetic data and for estimating parameters descriptive of the dominant vascular and tissue processes that determine lung uptake and accumulation of R6G, including $\Delta\psi_m$.

Hough et al. (JCI 4(3): e124329, 2019) used the fluorescent cationic dye tetramethylrhodamine ethyl ester (TMRE) to assess the effect of acute chemical lung injury on mitochondrial membrane potential of microvascular endothelial cells in isolated perfused mouse lungs. For that study, the lungs were loaded with TMRE by recirculated perfusate containing TMRE (2 μM) for 20 min, followed by a 10-min buffer washout. Acute chemical injury was then induced by microinfused concentrated hydrochloric acid (HCl) in the alveolar lumen using alveolar micro puncture technique. Confocal microscopy was used to measure TMRE fluorescent intensity in micro vessels in the injured local region before and after injury with HCl. Change in measured TMRE fluorescence was then used as measure of a change in $\Delta\psi_m$. Although this approach allows for assessing a change in endothelial TMRE fluorescence, it has many limitations. First, it provides a measure of local change in TMRE fluorescence, which may not be

reflective of the overall change in the lung. This especially true for many lung injury or disease, which is heterogeneous affecting some lung regions/lobes more than others. Second, a common pitfall in interpreting such data is that the logarithmic form of the Nernst equation specifies that changes in fluorescence intensity are not linearly proportional to changes in $\Delta\psi_m$. For instance, a 50% decrease in ratio to mitochondrial to cytosolic dye fluorescence translates to just 17% change in $\Delta\psi_m$. Third, this approach does not account for the fact that dyes such as TMRE are also Pgp substrates. For cell types that have few or no multidrug transporters, this may be of minimal importance, but multidrug transporters perform a key function in the pulmonary endothelium (Roerig et al., 2004). A change in Pgp activity will have an effect on TMRE mitochondrial fluorescence intensity. This effect could be misinterpreted to represent a change in $\Delta\psi_m$. Fourth, this approach requires loading the cells with TMRE by recirculating it through the lungs at a relatively high concentration (2 μM) for 20 min. TMRE accumulates in the mitochondrial matrix driven by $\Delta\psi_m$. The approach is confounded by the propensity of dyes such TMRE to undergo self-aggregation, quenching, and photobleaching and/or to exert phototoxic effects (Scaduto et al., 1999). This affects the utility of a change in measured mitochondrial TMRE fluorescence as an index of a change in $\Delta\psi_m$. The experimental and computational approach described in this thesis overcomes many of these limitations.

For the present study, the value of $\Delta\psi_p$ was fixed to that estimated by Gan et al. from cultured pulmonary endothelial cells (Gan et al., 2011). Previous studies have demonstrated a key role for $\Delta\psi_p$ in regulating channel-mediated calcium entry in response to mechanical stimuli, oxidative stress, ischemia, and hypoxia (Campbell et al.,

1991; Koliwad et al., 1996; Paffett et al., 2007; Stevens et al., 1994; Chatterjee et al., 2006). As such, $\Delta\psi_p$ could be altered by injury or disease. One could obtain information about $\Delta\psi_p$ by evaluating the impact of its depolarization on R6G lung uptake and retention. This could be done by perfusing the lungs with perfusate containing high potassium as was done by Gan et al. in cultured endothelial cells (Gan et al., 2011) or by Al-Mehdi et al. in isolated perfused rat lungs (Al-Mehdi et al., 1997). Another approach would be to use fluorescent dyes sensitive to $\Delta\psi_p$ such as the anionic probe bis-oxonol (Al-Mehdi et al., 1997; Zhang et al. 2005).

The lung vascular volume (V_e) was also fixed to that estimated from normal rat lungs (Audi et al., 2003). Lung injury, including oxidative stress, has been shown to change lung vascular and extravascular volumes (Audi et al. 2005; Crapo et al., 1980). An independent estimate of V_e could be obtained using lipophilic amines and indicator dilution methods in isolated perfused lungs as previously described (Audi et al., 2005; Ramakrishna et al., 2010).

The lung consists of 40 different resident cell types (Kotton et al., 2014; Dinh et al., 2017). The results using R6G provide no direct information regarding the contributions of the different cell types to the measured R6G lung uptake and estimated $\Delta\psi_m$, although endothelial cells would be expected to dominate because of their large surface area and high fraction (~50%) of total lung cells, and their direct contact with R6G in perfusate (Crapo et al., 1980). Although the question regarding the contributions of specific cell types will be important for future studies, alteration in the lung R6G uptake and estimated $\Delta\psi_m$ as an index of pulmonary mitochondrial dysfunction has functional implications regardless of the lung cell types involved.

We and others have reported various measures of mitochondrial dysfunction in intact lungs, pulmonary endothelial cells in culture, and isolated mitochondrial in response to oxidative stress (Gan et al., 2011; Audi et al., 2017; Sepehr et al., 2013; Gan et al., 2011; Ma et al., 2018; Audi et al., 2008; Merker et al., 2007; Pruijn et al., 1992). The proposed approach will allow us to quantify the effect of oxidative stress on $\Delta\psi_m$ in intact functioning lungs.

Preliminary results from lungs of rats exposed to hyperoxia show a decrease in R6G venous effluent concentration following the addition of FCCP. This suggest that the mitochondria in hyperoxic lungs is less coupled as compared to those in control lungs. This observation is consistent with the results from studies in mitochondria isolated from lungs of rats exposed to hyperoxia for 48 hours, which show a significant decrease in the activities of complex I and complex II, and prolonged ADP-stimulated $\Delta\psi_m$ depolarization (Audi et al., 2017). Experimental data in the presence of verapamil are needed to account for the effect of potential hyperoxia-induced change in Pgp activity on R6G venous effluent concentration.

6.2 Conclusions:

In conclusion, we present a novel experimental and computational approach for probing and estimating $\Delta\psi_m$ in intact lungs. The approach has the potential to provide quantitative assessment of the effect of various injurious conditions on lung mitochondrial function, and to evaluate the impact of therapies that target the mitochondria. The proposed approach can also be easily adapted for other organs or cationic dyes.

BIBLIOGRAPHY

Adams, D. J., & Hill, M. A. (2004). Potassium Channels and Membrane Potential in the Modulation of Intracellular Calcium in Vascular Endothelial Cells. Journal of Cardiovascular Electrophysiology, 15(5), 598-610. doi:10.1046/j.1540-8167.2004.03277.

Agard C, Rolli-Derkinderen M, Dumas-de-La-Roque E, Rio M, Sagan C, Savineau JP, Loirand G, Pacaud P. Protective role of the antidiabetic drug metformin against chronic experimental pulmonary hypertension. Br J Pharmacol. 2009;158(5):1285-94. PubMed PMID: 19814724.

Aiuchi, T., Daimatsu, T., Nakaya, K., & Nakamura, Y. (1982). Fluorescence changes of rhodamine 6G associated with changes in membrane potential in synaptosomes. Biochimica et Biophysica Acta (BBA) - Biomembranes, 685(3), 289-296. doi:10.1016/0005-2736(82)90070-0

Al-Jayyoussi, G., Price, D. F., Francombe, D., Taylor, G., Smith, M. W., Morris, C. Gumbleton, M. (2013). Selectivity in the impact of P-glycoprotein upon pulmonary absorption of airway-dosed substrates: A study in ex vivo lung models using chemical inhibition and genetic knockout. Journal of Pharmaceutical Sciences, 102(9), 3382-3394. doi:10.1002/jps.23587

Al-Mehdi, A., Shuman, H., & Fisher, A. B. (1997). Oxidant generation with K -induced depolarization in the isolated perfused lung. Free Radical Biology and Medicine, 23(1), 47-56. doi:10.1016/s0891-5849(96)00574-6

Altemeier, W. A., & Sinclair, S. E. (2007). Hyperoxia in the intensive care unit: why more is not always better. Current Opinion in Critical Care, 13(1), 73-78. doi:10.1097/mcc.0b013e32801162cb

Audi SH, Bongard RD, Dawson CA, Siegel D, Roerig DL, Merker MP. Duroquinone reduction during passage through the pulmonary circulation. Am J Physiol Lung Cell Mol Physiol. 2003;285(5):L1116-31. PubMed PMID: 12882764.

Audi SH, Bongard RD, Krenz GS, Rickaby DA, Haworth ST, Eisenhauer J, Roerig DL, Merker MP. Effect of chronic hyperoxic exposure on duroquinone reduction in adult rat lungs. Am J Physiol Lung Cell Mol Physiol. 2005;289(5):L788-97. PubMed PMID: 15994278.

Audi SH, Clough AV, Haworth ST, Medhora M, Ranji M, Densmore JC, Jacobs ER. 99MTc-Hexamethylpropyleneamine Oxime Imaging for Early Detection of Acute Lung Injury in Rats Exposed to Hyperoxia or Lipopolysaccharide Treatment. Shock. 2016;46(4):420-30. doi: 10.1097/SHK.0000000000000605. PubMed PMID: 26974426; PMCID: PMC5014734.

Audi SH, Friedly N, Dash RK, Beyer AM, Clough AV, Jacobs ER. Detection of hydrogen peroxide production in the isolated rat lung using Amplex red. Free Radic Res. 2018:1-11. doi: 10.1080/10715762.2018.1511051. PubMed PMID: 30175632.

Audi SH, Jacobs ER, Zhang X, Camara AK, Zhao M, Medhora MM, Rizzo B, Clough AV. Protection by Inhaled Hydrogen Therapy in a Rat Model of Acute Lung Injury Can be Tracked in vivo Using Molecular Imaging. Shock. 2017. doi: 10.1097/SHK.0000000000000872. PubMed PMID: 28403067.

Audi SH, Merker MP, Krenz GS, Ahuja T, Roerig DL, Bongard RD. Coenzyme Q1 redox metabolism during passage through the rat pulmonary circulation and the effect of hyperoxia. J Appl Physiol. 2008;105(4):1114-26. PubMed PMID: 18703762; PMCID: PMC2576032.

Baracca, A., Sgarbi, G., Solaini, G., & Lenaz, G. (2003). Rhodamine 123 as a probe of mitochondrial membrane potential: evaluation of proton flux through F0 during ATP synthesis. Biochimica et Biophysica Acta (BBA) - Bioenergetics, 1606(1-3), 137-146. doi:10.1016/s0005-2728(03)00110-5

Bassingthwaighte JB, Chaloupka M. Sensitivity functions in the estimation of parameters of cellular exchange. Fed Proc. 1984;43(2):181-4. PubMed PMID: 6692937; PMCID: PMC4132824.

Beard, D. A., Bassingthwaighte, J. B., & Greene, A. S. (2005). Computational modeling of physiological systems. Physiological Genomics, 23(1), 1-3. doi:10.1152/physiolgenomics.00117.2005

Beija, M., Afonso, C. A., & Martinho, J. M. (2009). ChemInform Abstract: Synthesis and Applications of Rhodamine Derivatives as Fluorescent Probes. ChemInform, 40(49). doi:10.1002/chin.200949242

Bongard, R. D., Yan, K., Hoffmann, R. G., Audi, S. H., Zhang, X., Lindemer, B. J., Merker, M. P. (2013). Depleted energy charge and increased pulmonary endothelial permeability induced by mitochondrial complex I inhibition are mitigated by coenzyme Q 1 in the isolated perfused rat lung. Free Radical Biology and Medicine,65: 1455-1463. doi:10.1016/j.freeradbiomed.2013.07.040

Bonora, M., Patergnani, S., Rimessi, A., De Marchi, E., Suski, J. M., Bononi, A., Giorgi, C., Marchi, S., Missiroli, S., Poletti, F., Wieckowski, M. R., ... Pinton, P. (2012). ATP synthesis and storage. Purinergic signalling, 8(3), 343-57. Doi:10.1007/s11302-012-9305-8

Campbell DL, Strauss HC, Whorton AR. Voltage dependence of bovine pulmonary artery endothelial cell function. J Mol Cell Cardiol. 1991;23 Suppl 1:133-44. PubMed PMID: 1903817.

Carraway, M. S., Suliman, H. B., Kliment, C., Welty-Wolf, K. E., Oury, T. D., & Piantadosi, C. A. (2008). Mitochondrial Biogenesis in the Pulmonary Vasculature During Inhalational Lung Injury and Fibrosis. Antioxidants & Redox Signaling, 10(2), 269-276. doi:10.1089/ars.2007.1910

Carvalho, C. R., Schettino, G. D., Maranh, B., & Bethlem, E. P. (1998). Hyperoxia and lung disease. Current Opinion in Pulmonary Medicine, 4(5), 300-304. doi:10.1097/00063198-199809000-00010

Cehovic, G. A., Hatton, K. W., & Fahy, B. G. (2009). Adult Respiratory Distress Syndrome. International Anesthesiology Clinics, 47(1), 83-95. doi:10.1097/aia.0b013e3181958a7d

Chatterjee S, Levitan I, Wei Z, Fisher AB. KATP channels are an important component of the shear-sensing mechanism in the pulmonary microvasculature. Microcirculation. 2006;13(8):633-44. doi: 10.1080/10739680600930255. PubMed PMID: 17085424.

Chen, L. (1988). Mitochondrial Membrane Potential In Living Cells. Annual Review of Cell and Developmental Biology, 4(1), 155-181. doi:10.1146/annurev.cellbio.4.1.155

Cho CW, Liu Y, Yan X, Henthorn T, Ng KY. Carrier-mediated uptake of rhodamine 123: implications on its use for MDR research. Biochem Biophys Res Commun. 2000;279(1):124-30. doi: 10.1006/bbrc.2000.3916. PubMed PMID: 11112427.

Chow, C., Abreu, M. T., Suzuki, T., & Downey, G. P. (2003). Oxidative Stress and Acute Lung Injury. American Journal of Respiratory Cell and Molecular Biology, 29(4), 427-431. doi:10.1165/rcmb.f278

Clark JM and Lambertsen CJ (1971). Pulmonary oxygen toxicity: a review. Pharmacol Rev 23: 37-133.

Clough, A. V., Audi, S. H., Haworth, S. T., & Roerig, D. L. (2012). Differential lung uptake of 99mTc-hexamethylpropyleneamine oxime and 99mTc-duramycin in the chronic hyperoxia rat model. J Nucl Med, 53(12), 1984-1991. doi:10.2967/jnumed.112.108498

Crapo, J. D., Barry, B. E., Foscue, H. A., & Shelburne, J. (1980). Structural and biochemical changes in rat lungs occurring during exposures to lethal and adaptive doses of oxygen. Am Rev Respir Dis, 122(1), 123-143. doi:10.1164/arrd.1980.122.1.123

Croxton, Thomas L. (2002). Future Research Directions in Chronic Obstructive Pulmonary Disease. Am. J. Respir. Crit Care Med. doi: 0.1164/ajrccm.165.6.2108036

Cunningham, C. C. (2004). Energy Availability and Alcohol–Related Liver Pathology. NIAAA. Retrieved May 08, 2018, from https://pubs.niaaa.nih.gov/publications/arh27-4/291-299.html

Davis, S, Weiss MJ, Wong JR, Lampidis TJ, Chen LB. (1985) Mitochondrial and plasma membrane potentials cause unusual accumulation and retention of Rhodamine 123 by human breast adenocarcinoma-derived MCF-7 cells. The Journal of Biological Chemistry, 260(25):13844-13850.

Dinh PC, Cores J, Hensley MT, Vandergriff AC, Tang J, Allen TA, Caranasos TG, Adler KB, Lobo LJ, Cheng K. Derivation of therapeutic lung spheroid cells from minimally invasive transbronchial pulmonary biopsies. Respir Res. 2017;18(1):132. doi: 10.1186/s12931-017-0611-0. PubMed PMID: 28666430; PMCID: PMC5493087.

Dorn, G. W. (2015). Mitochondrial dynamism and heart disease: Changing shape and shaping change. EMBO Molecular Medicine,7(7), 865-877. doi:10.15252/emmm.201404575

Duchen, M. R., Surin, A., & Jacobson, J. (2003). [17] Imaging mitochondrial function in intact cells. Methods in Enzymology Biophotonics, Part B, 353-389. doi:10.1016/s0076-6879(03)61019-0

Dutta S, Ebling WF. Parameter estimability of biphasic response models. J Pharm Sci. 1997;86(1):44-51. doi: 10.1021/js960248f. PubMed PMID: 9002458.

Ehrenberg, B., Montana, V., Wei, M., Wuskell, J., & Loew, L. (1988). Membrane potential can be determined in individual cells from the Nernstian distribution of cationic dyes. Biophysical Journal, 53(5), 785-794. doi:10.1016/s0006-3495(88)83158-8

Farkas, D., Wei, M., Febbroriello, P., Carson, J., & Loew, L. (1989). Simultaneous imaging of cell and mitochondrial membrane potentials. Biophysical Journal, 56(6), 1053-1069. doi:10.1016/s0006-3495(89)82754-7

Fisher, A. B. (1984). Intermediary metabolism of the lung. Environmental Health Perspectives, 55, 149-158. doi:10.1289/ehp.8455149

Fluorescence spectrometry. (n.d.). Retrieved June 05, 2017, from http://www.chromedia.org/chromedia?waxtrapp=mkqjtbEsHonOvmOlIEcCArB&subNav=cczbdbEsHonOvmOlIEcCArBP

Forster, S., Thumser, A. E., Hood, S. R., & Plant, N. (2012). Characterization of Rhodamine-123 as a Tracer Dye for Use In In vitro Drug Transport Assays. PLoS ONE, 7(3). Doi:10.1371/journal.pone.0033253

French, J. E. (1989). TOXICOLOGY AND CARCINOGENESIS STUDIES OF RHODAMINE 6G IN F344/N RATS AND B6C3F1 MICE (Technical Report Series, pp. 1-194, Rep. No. TR-364). Research Triangle Park, NC: National Toxicology Program.

Fu C, Dai X, Yang Y, Lin M, Cai Y, Cai S. Dexmedetomidine attenuates lipopolysaccharide-induced acute lung injury by inhibiting oxidative stress, mitochondrial dysfunction and apoptosis in rats. Mol Med Rep. 2017;15(1):131-8. doi: 10.3892/mmr.2016.6012. PubMed PMID: 27959438; PMCID: PMC5355722.

Gan Z, Roerig DL, Clough AV, Audi SH. Differential responses of targeted lung redox enzymes to rat exposure to 60 or 85% oxygen. J Appl Physiol. 2011;111(1):95-107. PubMed PMID: 21551015; PMCID: PMC3137546

Gan, Z., Audi, S. H., Bongard, R. D., Gauthier, K. M., & Merker, M. P. (2011). Quantifying mitochondrial and plasma membrane potentials in intact pulmonary arterial endothelial cells based on extracellular disposition of rhodamine dyes. AJP: Lung Cellular and Molecular Physiology, 300(5). doi:10.1152/ajplung.00334.2010

Gear, A. R. (1974). Rhodamine 6G: A Potent Inhibitor of Mitochondrial Oxidative Phosphorylation. The Journal of Biological Chemistry, 249(11), 3628-3637. Retrieved July 19, 2017.

Herasevich, V., Yilmaz, M., Khan, H., Hubmayr, R. D., & Gajic, O. (2009). Validation of an electronic surveillance system for acute lung injury. Intensive Care Medicine,35(6), 1018-1023. doi:10.1007/s00134-009-1460-1

Hough, R. F., Islam, M. N., Gusarova, G. A., Jin, G., Das, S., & Bhattacharya, J. (2019). Endothelial mitochondria determine rapid barrier failure in chemical lung injury. JCI insight, 4(3), e124329. Advance online publication. doi:10.1172/jci.insight.124329

Hu, S., Zhao, H., Yin, X. J., & Ma, J. K. (2007). Role of Mitochondria in Silica-Induced Apoptosis of Alveolar Macrophages: Inhibition of Apoptosis by Rhodamine 6g and N-acetyl-L-cysteine. Journal of Toxicology and Environmental Health, Part A, 70(17), 1403-1415. doi:10.1080/15287390701251990

Huang Y, Kwan KKL, Leung KW, Wang H, Kong XP, Dong TTX, Tsim KWK. The Extracts and Major Compounds Derived from Astragali Radix Alter Mitochondrial Bioenergetics in Cultured Cardiomyocytes: Comparison of Various Polar Solvents and Compounds. Int J Mol Sci. 2018;19(6). doi: 10.3390/ijms19061574. PubMed PMID: 29799462; PMCID: PMC6032251.

Huang, M., Camara, A. K., Stowe, D. F., Qi, F., & Beard, D. A. (2007). Mitochondrial Inner Membrane Electrophysiology Assessed by Rhodamine-123 Transport and Fluorescence. Annals of Biomedical Engineering, 35(7), 1276-1285. doi:10.1007/s10439-007-9265-2

Huber, H. J., Plchut, M., Weisová, P., Düssmann, H., Wenus, J., Rehm, M., Prehn, J. H. (2009). TOXI-SIM—A simulation tool for the analysis of mitochondrial and plasma

membrane potentials. Journal of Neuroscience Methods, 176(2), 270-275. doi:10.1016/j.jneumeth.2008.09.003

Hurd, S. (2000). The Impact of COPD on Lung Health Worldwide. Chest, 117(2). doi:10.1378/chest.117.2_suppl.1s

Johnson, E., Matthay, M. (2010). Acute Lung Injury: Epidemiology, Pathogensis, and Treatment. Journal of Aerosol Medicine and Pulmonary Drug Delivery, 23(4), 243-252. doi: 10.1089/jamp.2009.0775

Johnson, L. V., Walsh M.L., Bockus B.J., Chen L.B. (1981). Monitoring of relative mitochondrial membrane potential in living cells by fluorescence microscopy. The Journal of Cell Biology, 88(3), 526-535. doi:10.1083/jcb.88.3.526

Kalogeris, T., Bao, Y., & Korthuis, R. J. (2014). Mitochondrial reactive oxygen species: A double edged sword in ischemia/reperfusion vs. preconditioning. Redox Biology, 2, 702-714. doi: 10.1016/j.redox.2014.05.006

Koliwad SK, Kunze DL, Elliott SJ. Oxidant stress activates a non-selective cation channel responsible for membrane depolarization in calf vascular endothelial cells. J Physiol. 1996;491 (Pt 1):1-12. doi: 10.1113/jphysiol.1996.sp021191. PubMed PMID: 9011602; PMCID: PMC1158754.

Kotton DN, Morrisey EE. Lung regeneration: mechanisms, applications and emerging stem cell populations. Nat Med. 2014;20(8):822-32. doi: 10.1038/nm.3642. PubMed PMID: 25100528; PMCID: PMC4229034.

Levitt, J. E., & Matthay, M. A. (2012). Clinical review: Early treatment of acute lung injury--paradigm shift toward prevention and treatment prior to respiratory failure. Crit Care, 16(3), 223. doi:10.1186/cc11144

Lieu, P. B., Fornari, M., Ramos, T., Hatcher, A. S., & Clements-Jewery, H. (2011). Reduced Antiarrhythmic Efficacy of Verapamil in Isolated Rat Hearts in the Presence of Elevated Extracellular Calcium. Journal of Cardiovascular Pharmacology, 57(4), 455-462. doi:10.1097/fjc.0b013e31820ff60e

Liu, J. Q. (2006). A novel bronchial ring bioassay for the evaluation of small airway smooth muscle function in mice. AJP: Lung Cellular and Molecular Physiology, 291(2). doi:10.1152/ajplung.00320.2005

Loetchutinat C, Saengkhae C, Marbeuf-Gueye C, Garnier-Suillerot A. New insights into the P-glycoprotein-mediated effluxes of rhodamines. Eur J Biochem. 2003;270(3):476-85. doi: 10.1046/j.1432-1033.2003.03403.x. PubMed PMID: 12542697.

Ma C, Beyer AM, Durand M, Clough AV, Zhu D, Norwood Toro L, Terashvili M, Ebben JD, Hill RB, Audi SH, Medhora M, Jacobs ER. Hyperoxia Causes Mitochondrial Fragmentation in Pulmonary Endothelial Cells by Increasing Expression of Pro-

Fission Proteins. Arterioscler Thromb Vasc Biol. 2018;38(3):622-35. doi: 10.1161/ATVBAHA.117.310605. PubMed PMID: 29419407; PMCID: PMC5823793.

Mandalà, M., Serck-Hanssen, G., Martino, G., & Helle, K. B. (1999). The Fluorescent Cationic Dye Rhodamine 6G as a Probe for Membrane Potential in Bovine Aortic Endothelial Cells. Analytical Biochemistry, 274(1), 1-6. doi:10.1006/abio.1999.4253

Matthay, M. A., & Zemans, R. L. (2011). The acute respiratory distress syndrome: pathogenesis and treatment. Annu Rev Pathol, 6, 147-163. doi:10.1146/annurev-pathol-011110-130158

Matthay, M. A., & Zimmerman, G. A. (2005). Acute Lung Injury and the Acute Respiratory Distress Syndrome. American Journal of Respiratory Cell and Molecular Biology,33(4), 319-327. doi:10.1165/rcmb.f305

Merker MP, Audi SH, Lindemer BJ, Krenz GS, Bongard RD. Role of mitochondrial electron transport complex I in coenzyme Q1 reduction by intact pulmonary arterial endothelial cells and the effect of hyperoxia. Am J Physiol Lung Cell Mol Physiol. 2007;293(3):L809-19. PubMed PMID: 17601793.

Merker MP, Bongard, R.D., Gan, Z., and Audi, S.H. Mitochondrial Bioenergetics in Intact Normoxic and Hyperoxia-Adapted Pulmonary Arterial Endothelial Cells (BAEC). Free Radic Biol Med. 2009;47(Supplement 1):S98.

Morris, G., & Berk, M. (2015). The many roads to mitochondrial dysfunction in neuroimmune and neuropsychiatric disorders. BMC Medicine,13(1). doi:10.1186/s12916-015-0310-y

Mottram LF, Forbes S, Ackley BD, Peterson BR. Hydrophobic analogues of rhodamine B and rhodamine 101: potent fluorescent probes of mitochondria in living C. elegans. Beilstein J Org Chem. 2012;8:2156-65. doi: 10.3762/bjoc.8.243. PubMed PMID: 23365627; PMCID: PMC3554599.

Munch, G., Mckay, S., Gussakovsky, E., Kuzio, B., Kupriyanov, V. V., & Jilkina, O. (2011). Rhodamine 800 as a near-infrared fluorescent deposition flow tracer in rodent hearts. Journal of Biomedical Optics, 16(6), 065001. doi:10.1117/1.3583581

Murphy, M. (2009). How mitochondria produce reactive oxygen species. Biochemical Journal, 417(1), 1-13. doi:10.1042/bj20081386

Nsiah-Sefaa, A., & Mckenzie, M. (2016). Combined defects in oxidative phosphorylation and fatty acid β-oxidation in mitochondrial disease. Bioscience reports, 36(2). doi: 10.1042/bsr20150295

Nussbaum, R. L. (2005). Mining yeast in silico unearths a golden nugget for mitochondrial biology. Journal of Clinical Investigation,115(10), 2689-2691. doi:10.1172/jci26625

Paffett ML, Naik JS, Resta TC, Walker BR. Reduced store-operated Ca2+ entry in pulmonary endothelial cells from chronically hypoxic rats. Am J Physiol Lung Cell Mol Physiol. 2007;293(5):L1135-42. doi: 10.1152/ajplung.00432.2006. PubMed PMID: 17693482.

Perry, S., Norman, J., Barbieri, J., Brown, E., & Gelbard, H. (2011). Mitochondrial membrane potential probes and the proton gradient: A practical usage guide. BioTechniques,50(2), 98-115. doi:10.2144/000113610

Piantadosi CA, Suliman HB. Mitochondrial Dysfunction in Lung Pathogenesis. Annu Rev Physiol. 2017;79:495-515. doi: 10.1146/annurev-physiol-022516-034322. PubMed PMID: 27959621.

Pruijn FB, Schoonen WG, Joenje H. Inactivation of mitochondrial metabolism by hyperoxia-induced oxidative stress. Ann N Y Acad Sci. 1992;663:453-5. PubMed PMID: 1482084.

Ragaller, M., & Richter, T. (2010). Acute lung injury and acute respiratory distress syndrome. J Emerg Trauma Shock, 3(1), 43-51. doi:10.4103/0974-2700.58663

Ramakrishna M, Gan Z, Clough AV, Molthen RC, Roerig DL, Audi SH. Distribution of Capillary Transit Times in Isolated Lungs of Oxygen-Tolerant Rats. Ann Biomed Eng. 2010;38(11):3449-65. PubMed PMID: 20552277.

Roerig, D. L. (2004). Kinetic Characterization of P-Glycoprotein-Mediated Efflux of Rhodamine 6G in the Intact Rabbit Lung. Drug Metabolism and Disposition, 32(9), 953-958. doi:10.1124/dmd.104.000042

Rubenfeld GD, Caldwell E, Peabody E, Weaver J, Martin DP, et al. Incidence and outcomes of acute lung injury. N Engl J Med. 2005; 353:1685–93. [PubMed: 16236739]

Ruchko M, Gorodnya O, LeDoux SP, Alexeyev MF, Al-Mehdi AB, Gillespie MN. Mitochondrial DNA damage triggers mitochondrial dysfunction and apoptosis in oxidant-challenged lung endothelial cells. Am J Physiol Lung Cell Mol Physiol. 2005;288(3):L530-5. PubMed PMID: 15563690.

Ryter SW, Rosas IO, Owen CA, Martinez FJ, Choi ME, Lee CG, Elias JA, Choi AMK. Mitochondrial Dysfunction as a Pathogenic Mediator of Chronic Obstructive Pulmonary Disease and Idiopathic Pulmonary Fibrosis. Ann Am Thorac Soc. 2018;15(Supplement_4):S266-S72. doi: 10.1513/AnnalsATS.201808-585MG. PubMed PMID: 30759019.

Sasaki, S., Mccully, J. D., Alessandrini, F., & Locicero, J. (1995). Impact of initial flush potassium concentration on the adequacy of lung preservation. The Journal of Thoracic and Cardiovascular Surgery, 109(6), 1090-1096. doi:10.1016/s0022-5223(95)70192-3

Scaduto, R. C., & Grotyohann, L. W. (1999). Measurement of Mitochondrial Membrane Potential Using Fluorescent Rhodamine Derivatives. Biophysical Journal, 76(1), 469-477. doi:10.1016/s0006-3495(99)77214-0

Sepehr, R., Audi, S. H., Staniszewski, K. S., Haworth, S. T., Jacobs, E. R., & Ranji, M. (2013). Novel Fluorometric Tool to Assess Mitochondrial Redox State of Isolated Perfused Rat Lungs After Exposure to Hyperoxia. IEEE Journal of Translational Engineering in Health and Medicine, 1, 1500210-1500210. doi:10.1109/jtehm.2013.2285916

So, P. T., & Dong, C. Y. (2001). Fluorescence Spectrophotometry. Encyclopedia of Life Sciences. doi:10.1038/npg.els.0002978

Solaini, G., Sgarbi, G., Lenaz, G., & Baracca, A. (2007). Evaluating Mitochondrial Membrane Potential in Cells. Bioscience Reports, 27(1-3), 11-21. doi:10.1007/s10540-007-9033-4

Staniszewski, K., Audi, S. H., Sepehr, R., Jacobs, E. R., & Ranji, M. (2012). Surface Fluorescence Studies of Tissue Mitochondrial Redox State in Isolated Perfused Rat Lungs. Annals of Biomedical Engineering, 41(4), 827-836. doi:10.1007/s10439-012-0716-z

Stevens T, Cornfield DN, McMurtry IF, Rodman DM. Acute reductions in PO2 depolarize pulmonary artery endothelial cells and decrease [Ca2+]i. Am J Physiol. 1994;266(4 Pt 2):H1416-21. doi: 10.1152/ajpheart.1994.266.4.H1416. PubMed PMID: 8184919.

Ten VS, Ratner V. Mitochondrial bioenergetics and pulmonary dysfunction: Current progress and future directions. Paediatr Respir Rev. 2019. doi: 10.1016/j.prrv.2019.04.001. PubMed PMID: 31060947.

Thaler, S., Haritoglou, C., Choragiewicz, T. J., Messias, A., Baryluk, A., May, C. A., Schuettauf, F. (2008). In Vivo Toxicity Study of Rhodamine 6G in the Rat Retina. Investigative Opthalmology & Visual Science, 49(5), 2120. doi:10.1167/iovs.07-1476

Vogel, R., Meredith, P., Harvey, M., & Rubinsztein-Dunlop, H. (2004). Absorption and fluorescence spectroscopy of rhodamine 6G in titanium dioxide nanocomposites. Spectrochimica Acta Part A: Molecular and Biomolecular Spectroscopy,60(1-2), 245-249. doi:10.1016/s1386-1425(03)00218-x

Wheeler, A. P., & Bernard, G. R. (2007). Acute lung injury and the acute respiratory distress syndrome: a clinical review. Lancet, 369(9572), 1553-1564. doi:10.1016/S0140-6736(07)60604-7

Williams, A., Murrel, M., Brammah, S., Minchenko, J., & Christodoulou., J. (1999). A Novel System for Assigning the Mode of Inheritance in mitochondrial Disorders Using Cybrids and Rhodamine 6G. Human Molecular Genetics, 8(9): 1691-1697. 10.1093/hmg/8.9.1691

Xiao Zhang dissertation proposal: Thermodynamically-Constrained Computational Modeling of lung tissue bioenergetics and the effect of hyperoxia-induced acute lung injury

Yuan, C., Gao, J., Guo, J., Bai, L., Marshall, C., Cai, Z., . . . Xiao, M. (2014). Dimethyl Sulfoxide Damages Mitochondrial Integrity and Membrane Potential in Cultured Astrocytes. PLoS ONE, 9(9). doi:10.1371/journal.pone.0107447

Zehentbauer, F. M., Moretto, C., Stephen, R., Thevar, T., Gilchrist, J. R., Pokrajac, D., Kiefer, J. (2014). Fluorescence spectroscopy of Rhodamine 6G: Concentration and solvent effects. Spectrochimica Acta Part A: Molecular and Biomolecular Spectroscopy, 121, 147-151. doi:10.1016/j.saa.2013.10.062

Zhang Q, Matsuzaki I, Chatterjee S, Fisher AB. Activation of endothelial NADPH oxidase during normoxic lung ischemia is KATP channel dependent. Am J Physiol Lung Cell Mol Physiol. 2005;289(6):L954-61. doi: 10.1152/ajplung.00210.2005. PubMed PMID: 16280460.

Zhao Z, Gordan R, Wen H, Fefelova N, Zang WJ, Xie LH. Modulation of intracellular calcium waves and triggered activities by mitochondrial ca flux in mouse cardiomyocytes. PLoS One. 2013;8(11):e80574. doi: 10.1371/journal.pone.0080574. PubMed PMID: 24348912; PMCID: PMC3857829.

APPENDIX

A. Preparation of Stock solutions:

A.1 FCCP Preparation and Fractionation:

Molecular Weight of FCCP: 254.17 g

DMSO Solubility: Up to 10 mM

We have a 10 mg bottle of FCCP

For a 100 μM stock of FCCP, what volume of DMSO is needed?

- 1 mole of FCCP → 254.17 g
- ? → $10 * 10^{-3}$ g

$$x = \frac{10*10^{-3} g*mol}{254.17\ g} = 0.03934\ mmol \quad \text{(A.1.1)}$$

$$100\ mM = \frac{0.03934\ mmol}{x} \quad \text{(A.1.2)}$$

$$x = \frac{0.03934\ mmol}{100\ \frac{mmol}{L}} = 0.3934\ mL \quad \text{(A.1.3)}$$

For a perfusate concentration of 50 μM FCCP:

- Reservoir volume is 25 mL
- Add 12.5 μL (0.05% DMSO) of stock per 25 mL in reservoir for a final concentration of 50 μM

Stock Fractionation:

- 10 mg → 0.3934 mL DMSO
- Fractionate → 25 μL volumes
- This gives us a total of 15 vials we can use
- Freeze

A.2 Verapamil HCL Preparation:

Important Information:

- Molecular Weight = 491.069 g/mol
- Soluble in H_2O (83 mg/mL)
- Previous study used 0.1 mM

1.) 5 mg = 10.18 umol in 10 mL DH2O = 1.018 mM

2.) Or add 5 mg to 100 mL perfusate for final concentration of 0.1 mM

A.3 Preparation of Perfusate:

0.5% BSA and 2.5% Ficoll

i. Take BSA jar first out of fridge to cool down before opening it.
ii. Prepare a bottle of DH_2O.
iii. Take a beaker with the proper volume, label it, and add a stirring stick into it. Then Add a proper volume of DH_2O, the amount is the total volume minus 50 mL for each 300 mL.
iv. Place the beaker on the heater, set the stir as '2' **(no heat)**.
v. Calculate/add the following chemicals required, for 100 mL (0.5% BSA 2.5% Ficoll),

Add stock **in order**, weigh the assigned quantity of stuffs, and add them into the beaker						
Stock (in Fridge)	**KCL**, 0.5 mL	**$CaCl_2$** , 0.5 mL	**$MgSO_4$** , 0.5 mL	**KH_2PO_4** , 0.5 mL		
Chemicals (on the shelves) **Note: use separate spatula for each chemical**	**NaCl**, 0.69 g	**Dextrose**, 0.1 g	**Sodium Bicarbonate**, 0.21 g	**BSA**, 0.5 g	**Papaverine**, 0.06 g	**Ficoll**, 2.5 g

Note: Please keep the table clean always. Clean the electronic balance after all stuffs have been weighed.

Note: Papaverine is used as a vasodilator to prevent smooth muscle cells within the lung from constricting and therefore increasing pressure which in turn leads to edema and tissue death.

Note: Addition of Papaverine slightly lowers the pH value.

vi. Take a glass stir bar and push BSA into solution.
vii. Put a piece of parafilm on to cover the beaker to prevent contamination and to keep it stirring until all BSA is in solution (15-20 min).
viii. Use a graduated cylinder to bring the solution to the desired volume and then place the solution into a clean saline bottle with labels including date and contents.

Note: Place the label on the shoulder of the bottle to prevent from getting wet.

ix. Empty the beaker content into a plastic bottle. Use a cone (with a cotton gauze to filter out any particulate in the Perfusate).
x. Place the bottle into the warm water bath (37 °C) for ten minutes.
xi. Prepare the gas mixture in the balloon.

a.) Take a gas balloon.
b.) Turn on all the tanks, using fine adjustment valves to set the parameter as **(settings of stainless steel balls)** N_2=7, O_2=38, CO_2=120.
c.) Close the three-way stopcock to the balloon and begin filling the balloon with the gas mixture for about 5 minutes. Then insert a cork into the tubing and **turn off all the tanks.**
d.) Withdraw a syringe of mixture gas in the balloon, and check the gas ingredients with the blood gas analyzer. **Reference value:** O_2: 16%, CO_2: 5%.
e.) Cut the tubing long enough to reach from the pump to the bottom of bottle, turn the three-way valve open to the balloon.
f.) Allow the gas mixture to bubble for about 20 minutes, check the pH at intervals – use a syringe with long needle, withdraw about 1 mL and check the pH with the blood gas analyzer. **Reference Value:** O_2:120-140 mmHg, Co_2: 35-40 mmHg and pH: 7.4.

Note: If the pH is high, then keep bubbling, if the pH is too low, then prepare for another gas balloon without CO_2 and bubble the Perfusate with this gas mixture.

g.) When BSA is ready, begin to prepare for other stuffs and the perfusion system.

$$CO_2 + H_2O \leftrightarrow H_2CO_3 \leftrightarrow HCO_3^- + H^+$$

<u>Law of pH</u>

>7.4: too little hydrogen and too much CO_2

- bubble w/ CO_2 **to drive reaction.**

<7.4: too much hydrogen and too little CO_2

- bubble w/ air **to drive reaction.**

A.4 R6G Stock Procedure**:**

Note: Prepare and use solutions on the same day. However, if there is a need to make up stock solutions in advance, it is recommended that you store the solution as aliquots in tightly sealed vials at -20°C. These solutions will be viable for up to one month. Allow the solution to equilibrate to room temperature for at least 1 hour before using.

- Molecular weight of R6G: 479.02 g/mole
- Mix 1 mg R6G powder with 1 mL H_2O to make **Stock 1**
  - This yields a concentration of 2.09 mM
- Then dilute by taking 40 uL of the stock and add it to 1.96 mL H_2O to make **Stock 2**
  - This gives a stock concentration of 41.8 uM
  - Now add 0.7177 mL of **Stock 2** to 120 mL perfusate to get an R6G concentration of 0.25 uM in the perfusate

B. PTI Software Setup:

1) Open the Felix software.
2) Select the Rhodamine 6G macro.
3) Select 'Set up'.
4) Select 'Time based'
5) Select the acquisition settings tab in the set-up window.
6) Switch the excitation wavelength to 525 nm.
7) Change the acquisition time to 2000 seconds.

C. Experimental setup/procedure:

R6G Single Pass Experiment

Materials Needed:

- Dark marker for labeling
- One beaker labeled for perfusate only
- One beaker labeled for R6G and perfusate
- One beaker labeled for R6G, perfusate, and verapamil
- Plastic beaker for waste
- One beaker and one squirt bottle for deionized water

- Large and smalls syringes with tubing for rinsing cuvette
- R6G stock
- Verapamil and/or FCCP
- 2.5% Ficoll-Krebs/0.5% BSA perfusate
- (74 - 1.7mL) Eppendorf tubes for samples to be centrifuged in
  - 42 for single pass, 8 for wash, and 24 for uncoupler. Have extras on hand.
- Micropipettes (two P1000's for 717.7 μL and 1000 μL and one P200 for FCCP)
- Labels for eppendorf tubes **need to be the same as timer** (no time for conversions during experiment)
- Stirring rod
- Extra eppendorf holder for eppendorfs used during collection
- Cuvette vacuum cleaner device

Methods:

Excitation Wavelength: 525 nm

Emission Wavelength: 565 nm

Notes: Then take the cuvette measurements at the end of the experiment. Make sure all equipment is turned on and warmed up 30 minutes prior to experiment (i.e. water bath). Practice time callouts before IPRL experiment.

If using Verapamil:

- Wash with regular perfusate for 5 minutes to rinse out any R6G and/or blood
- Add Verapamil to perfusate without R6G
- Flow: 10 mL/min
- Recirculate for 3 minutes
- Then turn the pump off
- Drain the perfusate
- Begin procedure below but add verapamil perfusate to the system

If not using Verapamil:

- Turn pump off
- Add 717.7 μL R6G stock to 120 mL perfusate (0.02 mg/mL) = 0.25 μM
- Stir with glass stirring rod
- Add perfusate w/o R6G to reservoir
- Take "Background" sample now from the normal perfusate (use 2 - 1.7 mL eppendorf tubes)
- Drain the perfusate w/o R6G from the reservoir

- Add 50 mL perfusate w/R6G to the reservoir then continuously add more to keep reservoir from becoming empty and allowing air to enter the system
- Take "0" sample now (use 2 - 1.7 mL eppendorf tubes)
- Turn pump on
- Draw samples out at 40 seconds, 60 seconds, 1:20, 1:40, 2, 2:20, 2:40, 3, 3:20, 3:40, 4, 4:20, 4:40, 5, 6, 7, 8, 9 and 10 minutes (use 2 - 1.7 mL eppendorf tubes per sample time)
- With flow rate of 10 mL/min fill tubes for 6 seconds each.
  - Do this by taking samples 6 seconds before and after the times stated above.
- Stop the flow and wash the reservoir (perform this as quickly as possible).
- Rinse the system/lung for 3 minutes (single pass) with perfusate without R6G.
  - Make sure to get a new baseline for each new condition (i.e. wash) before turning the pump back on.
  - Measure for 3 minutes taking samples at 1, 2, and 3 minutes (use 2 - 1.7 mL eppendorf tubes per sample time)
- Stop the flow and wash the reservoir (perform this as quickly as possible).
- Next add the uncoupler (FCCP) to perfusate without R6G and measure the effects.
  - Make sure to get a new baseline for each new condition (i.e. FCCP) before turning the pump back on.
  - Measure for 7 minutes taking samples at 13:20, 13:40, 14, 14:20, 14:40, 15, 16, 17, 18, 19, and 20 minutes (use 2 - 1.7 mL eppendorf tubes per sample time)
- All samples are spun for 1 minute in the centrifuge @ 10.5 x 1,000 RPM @ 4°C
- Add each time sample (from 2 eppendorf tubes) to a single cuvette and measure for fluorescence.
- Make sure to use only **one cuvette but rinse** it with deionized water before taking any measurements.

D. Standard Curve:

Materials Needed:

- Cuvette
- Micropipettes (two P1000's for 1 mL and 0.25 mL, one p5000 for 2.25 mL, and one P100 for 53.82 μL)
- 5 large tubes for doing the mixing/dilution
- 2.5% Ficoll-Krebs/0.5% BSA perfusate
- (12 - 1.7mL) Eppendorf tubes for samples to be centrifuged in
- Labels for eppendorf tubes
- Extra eppendorf holder for collection eppendorfs

Methods:

- Get "zero" sample of perfusate without R6G
- Add 53.82 μL of R6G **Stock 2** to 4.5 mL of perfusate in a large tube to get a concentration of 0.5 μM
- Dilute by taking 2.25 mL of the perfusate w/ R6G and mixing it with 2.25 mL of the perfusate w/o R6G to get a concentration of 0.25 μM
- Dilute by taking 2.25 mL of the previous perfusate w/ R6G and mixing it with 2.25 mL of the perfusate w/o R6G to get a concentration of 0.125 μM
- Dilute by taking 2.25 mL of the previous perfusate w/ R6G and mixing it with 2.25 mL of the perfusate w/o R6G to get a concentration of 0.0625 μM
- Dilute by taking 2.25 mL of the previous perfusate w/ R6G and mixing it with 2.25 mL of the perfusate w/o R6G to get a concentration of 0.03125 μM
- Now place 1 mL in each eppendorf tube (2) per concentration
- Then place them symmetrically in the centrifuge for 1 minute @ 10. 5 x 1,000 RPM @ 4^{o}C
- Use **single** cuvette and **rinse** before each measurement with deionized water
- Make sure to **start with lowest concentrations first** and end with highest concentrations to avoid harmful binding effects
- Place supernatant (from 2 eppendorf tubes per concentration) into cuvette and take sample of fluorescence
- Use data to create standard curve in sigma plot or excel

E. Matlab Code:

E.1 r6g_single_pass_sim.m

```
function r6g_single_pass_sim
%%
clear all
close all
clc
global deltap F
%% Values of model parameters
vmaxkm = 13.989154; %18.7;% Kpgp Rate of efflux of R6G from pgp pump (ml/min)
k2_bar = 11.147875;% Apparent rate constant for R6G-Bc binding within the cytoplasm region(min-1)
kminus2 = 0.093307;%Dissociation rate constant of R6G-Bc binding within the cytoplasm region (uM-1*min-1)
kd3 = 0.019121;%Dissociation equilibrium constant for dye-protein binding in the mitochondria region (umol-1*min-1)
```

```
ps2 = 0.837797;% dye permeability-surface area product across mitochondria
membrane (ml/min)
deltam = 122.558453; % Mitochondrial membrane potential (mV)
deltam_un =0.1; %68; % mitochondrial membrane potential after uncoupler is
added (mV)

%fixed
deltap = 43; %40 Plasma membrane potential (mV)
F = 10; %Flow (ml/min)
%%---------------
% plot(tt,blood_tissue_region)
Ce_bar = 0; %Total initial vascular R6G concentration (uM)
Cc = 0; %Total initial tissue R6G concentration (uM)
Cm = 0; %Total initial mitochondrial R6G concentration (uM)
CcBc = 0; % Total intial bound r6g cytoplasm concentration (uM)
Ctub1 = 0; % Total intial tubing r6g concentration (uM)
%Ctub2 = 0; % Total intial tubing r6g concentration (uM)
%Ctub3 = 0; % Total intial tubing r6g concentration (uM)
%Ctub4 = 0; % Total intial tubing r6g concentration (uM)
% show the values of parameters during optimization process
% parameter_values = p;
parameter_values(1) = ps2;
parameter_values(2) = k2_bar;
parameter_values(3) = kminus2;
parameter_values(4) = kd3;
parameter_values(5) = deltam;
parameter_values(6) = deltam_un;
parameter_values(7) = vmaxkm;


%% calling to function solving ODE's
ttdata = [0:0.1:20]';
options=odeset('InitialStep',1e-10,'RelTol',1e-10,'Refine',-
1);%,'NormControl','on');

% temp = parameter_values;
x0 = [Ctub1 Ce_bar Cc Cm CcBc]; % mass/volume aka concentration input
calculated based off real experimental values (uM)

% calling to ode
[tfinal,xfinal] = ode45(@r6g_odes, ttdata, x0, options, parameter_values);

%% open file, read experimental data to be fit
figure
plot(tfinal, xfinal(:,2), ttdata, xfinal(:,2))
```

```
infile = 'sim.txt';
 fid = fopen(infile, 'w');
%% read data from fil

for i=1:length(ttdata)
fprintf(fid,'%f %f\n', tfinal(i), xfinal(i,2));
end
 fclose(fid);
%get data
```

E.2 r6g_odes.m

```
function [ x_dot ] = r6g_odes(ttdata,x, parameters)

global deltap F

% define parameters
Ve = 0.85; %Physical lung vascular volume = 1 ml
Vc = 1; %Physical lung tissue volume = 1 ml
Vm = 0.02*Vc; %Physical lung mitochondrial volume = 0.01*Vc (ml)
Vtub = 4; % measured Physical tubing volume (ml)
alpha = 0.0374158; %ZF/RT   where Z is the valency of the ions (Na+, Ca2+, and
Cl-), F is Faraday's constant ...
...(9.684 x 104 C/ mol), R is the gas constant (8.135 J/K*mol), and T is the
absolute temperature in K (273 + temp in Celcius). (mV-1)
Be = 0.5; %[BSA]    Total vascular protein (BSA) concentration (uM)
kd1 = 0.32;%15; %k-1/k1   %Dissociation equilibrium constant for dye-protein
binding in the vascular region (umol-1*min-1)
ps1 = 50.558129;

%%%%%%%%%%%%%%%%
ps2         = parameters(1);
k2_bar      = parameters(2);
kminus2     = parameters(3);
kd3         = parameters(4);
deltam      = parameters(5);
deltam_un   = parameters(6);
vmaxkm      = parameters(7);

% calculate the apparent volumes
V3 = Vm*(1+(1/kd3));    %Apparent mitochondrial volume (ml)

%create vector of zeros
x_dot = zeros(5,1);

% get last time point from data gathered
time = 20;
```

```
% varying Cin based off phase and deltam
if ttdata >= 0 && ttdata <= (time-9.6) % phase 1... loading phase
   Cin = 0.25;
elseif ttdata > (time-9.6) && ttdata <= (time-6.6) % phase 2... wash phase
   Cin = 0;
elseif ttdata > (time-6.6) % phase 3... uncoupler phase
   Cin = 0;
   deltam = deltam_un;     %Mitochondrial membrane potential (mV)
end

% Free concentration of r6g within the vascular region
Ce = (x(2)/(1+(Be)/(kd1))); %units = nmol/mL or umol/L

% calculate flux values
J1 = ((alpha*ps1*deltap)/(exp(alpha*deltap)-1))*(exp(alpha*deltap)*Ce-x(3));
%Dye flux across plasma membrane (nmol/min)
J2 = ((alpha*ps2*deltam)/(exp(alpha*deltam)-1))*(exp(alpha*deltam)*x(3)-x(4));
%Dye flux across inner mitochondrial membrane (nmol/min)

% ODE's - do differential computations here
x_dot(1,1) = (1.0/(Vtub))*F*(Cin-x(1)); % tubing region
x_dot(2,1) = (1/Ve)*(-J1+vmaxkm*x(3)+F*(x(1)-x(2))); % extracellular/vascular
region units = nmol/mL*min
x_dot(3,1) = kminus2*x(5)-k2_bar*x(3)+(1/Vc)*(J1-J2-vmaxkm*x(3)); %
cytoplasm region free
x_dot(4,1) = (1/V3)*(J2); % mitochondrial region units = nmol/mL*min
x_dot(5,1) = k2_bar*x(3)-kminus2*x(5); % cytoplasm region bound

end
```

E.3 r6g_fit_v3_single.m

```
function r6g_fit_v3

% % initial cleanup
clear all
close all
clc

global deltap F tt deltam_un
 %% open file, read experimental data to be fit
infile = 'conc_data_041018.txt';
  fid = fopen(infile, 'r');
%% read data from file
 data150 = textscan(fid,'%f %f');
 fclose(fid);
```

```
%get data
  tt = (data150{1});
 blood_tissue_region=(data150{2});

% plot(tt,blood_tissue_region)
figure
plot(tt, blood_tissue_region)

%% initialize and do lsqcurvefit

    % define the data which will be used to estimate parameters
    indata = [blood_tissue_region];

    % define the corresponding sampling time points
    ttdata = [tt];

%%%%%
 figure
     subplot(2,1,1)
     plot(ttdata,indata,'ko')
%     legend('Data','Fitted Curve')
     title('Data and Fitted Curve from Residuals')
     xlabel('Time (minutes)')
     ylabel('Concentration (uM)')

hold on
for i =1:1
%% define initial values for the unknown parameters
vmaxkm = 8.840851;% Kpgp Rate of efflux of R6G from pgp pump (ml/min)
k2_bar = 12.475779;% Apparent rate constant for R6G-Bc binding within the
cytoplasm region(min-1)
kminus2 = 0.110531;%Dissociation rate constant of R6G-Bc binding within the
cytoplasm region (uM-1*min-1)
kd3 = 0.02313;%Dissociation equilibrium constant for dye-protein binding in the
mitochondria region (umol-1*min-1)
ps2 = 0.83082;% dye permeability-surface area product across mitochondria
membrane (ml/min)
deltam = 123.11; % Mitochondrial membrane potential (mV)
deltam_un = 0.1; % mitochondrial membrane potential after uncoupler is added
(mV)
ps1 = 49.4309;
%fixed
deltap = 43; %40 Plasma membrane potential (mV)
F = 10; %Flow (ml/min)
```

```
    % define the optimization options
    options = optimset('Algorithm', 'trust-region-reflective', 'MaxFunEvals', 3000,
'TolFun', 1e-15,'TolX',1e-10);

%% no verapamil fitting
 % define the parameters which will be estimated
    p0 = [ps2, k2_bar, kminus2, kd3, deltam, vmaxkm, ps1];

    % define the lower bound of parameters
    %lb = 0.0001*ones(length(p0),1);
    lb = [0.0001, 0.0001, 0.0001, 0.0001, 110, 0, 0.001];

    % define the upper bound of parameters
   % ub = [200 200 200 200 200 200 1  200];%
    ub = 300*ones(length(p0),1); %[20 20 20 20 20 20];
% fitting model to input data and find out the optimized values for parameters
[p, ssd, residual, ef, outt,lambda, jacobian] =
lsqcurvefit(@r6g_single_pass_param_est_v3, p0, ttdata, indata, lb, ub, options);
%%%%%%
PPAR(i,1) = p(1);
PPAR(i,2) = p(2);
PPAR(i,3) = p(3);
PPAR(i,4) = p(4);
PPAR(i,5) = p(5);
PPAR(i,6) = p(6);
PPAR(i,7) = p(7);

fit_conc = indata+residual;

     plot(ttdata, fit_conc,'b-')


end
p(1) = mean(PPAR(:,1))
p(2) = mean(PPAR(:,2))
p(3) = mean(PPAR(:,3))
p(4) = mean(PPAR(:,4))
p(5) = mean(PPAR(:,5))
p(6) = mean(PPAR(:,6))
p(7) = mean(PPAR(:,7))

%%%%%%
PPAR(:,1)
PPAR(:,2)
PPAR(:,3)
PPAR(:,4)
```

```
PPAR(:,5)
PPAR(:,6)
PPAR(:,7)
   % residual = model fit - data

   %
   %correlation matrix
NP = length(p0);
h = inv(jacobian'*jacobian);
for i = 1:NP;
 for j = 1:NP;
 cc(i,j) = h(i,j)/((h(i,i)*h(j,j))^0.5);
 end
end
full(cc)

%confidence intervals (95% confidence, alpha = 0.05)
s_2 = ssd/(length(indata) - NP);
for i = 1:NP;
 seb(i) = ((s_2)^0.5)*(h(i,i)^0.5);
end
alpha = 0.05;
tt_dis = - tinv(alpha/2, length(indata) - length(p0)); % tinv is the Student's t
inverse cumulative

%distribution function
seb = seb.*tt_dis;
seb
%%%%%%%%

    figure
    plot(ttdata, jacobian(:,1))
%   figure
%    plot(ttdata, jacobian(:,2))
%    figure
%    plot(ttdata, jacobian(:,3))
%    figure
%    plot(ttdata, jacobian(:,4))
    figure
    plot(ttdata, jacobian(:,5))
%    figure
%    plot(ttdata, jacobian(:,6))
%    figure
%    plot(ttdata, jacobian(:,7))
%    figure
```

```
    % display the optimized values of parameters and related results
%     fprintf('result:\n   PS1 = %f +/- %f ml/min\n', p(1), ci(1,1));
    fprintf('   PS2 = %f ml/min\n', p(1));
%     fprintf('   kd1 = %f +/- %f Percent BSA\n', p(3), ci(1,3));
    fprintf('   k2_bar = %f min-1\n', p(2));
    fprintf('   kminus2 = %f min-1\n', p(3));
    fprintf('   kd3 = %f  uM\n', p(4));
    fprintf('   deltam = %f mV\n', p(5));
   % fprintf('   deltam_un = %f  mV\n', p(6));
    fprintf('   VmaxKm = %f ml/min\n', p(6));
      fprintf('   ps1 = %f ml/min\n', p(7));
%     fprintf('   deltap = %f +/- %f mV\n', p(8), ci(1,8));
    fprintf('   deltap = %f mV\n', deltap);
    fprintf('   SSD = %f\n', ssd);

    end
```

E.4 r6g_single_pass_param_est_v3.m

```
function Out = r6g_single_pass_param_est_v3(p, ttdata)

global deltap F tt deltam_un

%% Initial values for ODEs

Ce_bar = 0; %Total initial vascular R6G concentration (uM)
Cc = 0; %Total initial tissue R6G concentration (uM)
Cm = 0; %Total initial mitochondrial R6G concentration (uM)
CcBc = 0; % Total intial bound r6g cytoplasm concentration (uM)
Ctub1 = 0; % Total intial tubing r6g concentration (uM)
%Ctub2 = 0; % Total intial tubing r6g concentration (uM)
%Ctub3 = 0; % Total intial tubing r6g concentration (uM)
%Ctub4 = 0; % Total intial tubing r6g concentration (uM)
% show the values of parameters during optimization process
% parameter_values = p;
parameter_values(1) = p(1);
parameter_values(2) = p(2);
parameter_values(3) = p(3);
parameter_values(4) = p(4);
parameter_values(5) = p(5);
parameter_values(6) = p(6);
parameter_values(7) = p(7);
%parameter_values(8) = p(8);

%% calling to function solving ODE's
```

```
options=odeset('InitialStep',1e-10,'RelTol',1e-10,'Refine',-
1);%,'NormControl','on');

% temp = parameter_values;
x0 = [Ctub1 Ce_bar Cc Cm CcBc]; % mass/volume aka concentration input
calculated based off real experimental values (uM)

% calling to ode
[tfinal,xfinal] = ode45(@rhodamine6GSolver_single_pass_param_est_v3, ttdata,
x0, options, parameter_values);

Out = xfinal(:,2);
```

E.5 rhodamine6GSolver_single_pass_param_est_v3.m

```
function [ x_dot ] = rhodamine6GSolver_single_pass_param_est_v3(ttdata,x,
parameters)

global deltap F tt deltam_un

% define parameters
Ve = 0.85; %Physical lung vascular volume = 1 ml
Vc = 1.0; %0.67; %Physical lung tissue volume = 1 ml
Vm = 0.02*Vc; %Physical lung mitochondrial volume = 0.01*Vc (ml)
Vtub = 4; % measured Physical tubing volume (ml)
alpha = 0.0374158; %ZF/RT   where Z is the valency of the ions (Na+, Ca2+, and
Cl-), F is Faraday's constant ...
...(9.684 x 104 C/ mol), R is the gas constant (8.135 J/K*mol), and T is the
absolute temperature in K (273 + temp in Celcius). (mV-1)
Be = 0.5; %[BSA]    Total vascular protein (BSA) concentration (uM)
kd1 = 0.32; %0.306430;%15; %k-1/k1   %Dissociation equilibrium constant for
dye-protein binding in the vascular region (umol-1*min-1)
%ps1 = 63.551726;

%%%%%%%%%%%%%%%%
ps2         = parameters(1);
k2_bar      = parameters(2);
kminus2     = parameters(3);
kd3         = parameters(4);
deltam      = parameters(5);
%deltam_un   = parameters(6);
vmaxkm      = parameters(6);
ps1         = parameters(7);
% calculate the apparent volumes
V3 = Vm*(1+(1/kd3));    %Apparent mitochondrial volume (ml)

%create vector of zeros
```

```
x_dot = zeros(5,1);

% get last time point from data gathered
time = tt(end);

% varying Cin based off phase and deltam
if ttdata >= 0 && ttdata <= (time-9.6) % phase 1... loading phase
   Cin = 0.25;
elseif ttdata > (time-9.6) && ttdata <= (time-6.6) % phase 2... wash phase
   Cin = 0;
elseif ttdata > (time-6.6) % phase 3... uncoupler phase
   Cin = 0;
   deltam = deltam_un;     %Mitochondrial membrane potential (mV)
end

% Free concentration of r6g within the vascular region
Ce = (x(2)/(1+(Be)/(kd1))); %units = nmol/mL or umol/L

% calculate flux values
J1 = ((alpha*ps1*deltap)/(exp(alpha*deltap)-1))*(exp(alpha*deltap)*Ce-x(3));
%Dye flux across plasma membrane (nmol/min)
J2 = ((alpha*ps2*deltam)/(exp(alpha*deltam)-1))*(exp(alpha*deltam)*x(3)-x(4));
%Dye flux across inner mitochondrial membrane (nmol/min)

% ODE's - do differential computations here
x_dot(1,1) = (1.0/(Vtub))*F*(Cin-x(1)); % tubing region
x_dot(2,1) = (1/Ve)*(-J1+vmaxkm*x(3)+F*(x(1)-x(2))); % extracellular/vascular
region units = nmol/mL*min
x_dot(3,1) = kminus2*x(5)-k2_bar*x(3)+(1/Vc)*(J1-J2-vmaxkm*x(3)); %
cytoplasm region free
x_dot(4,1) = (1/V3)*(J2); % mitochondrial region units = nmol/mL*min
x_dot(5,1) = k2_bar*x(3)-kminus2*x(5); % cytoplasm region bound

end
```